Li, Zhao; Bai, Yujiao; Shin, G. Kang; Yan, Zheng; Li, Hui

Inside-Out Precoding to Manage Multiple Interferences from the Same Source

Published in:
IEEE Transactions on Vehicular Technology

DOI:
10.1109/TVT.2020.2994332

Published: 01/07/2020

Document Version
Peer reviewed version

Please cite the original version:
Li, Z., Bai, Y., Shin, G. K., Yan, Z., & Li, H. (2020). Inside-Out Precoding to Manage Multiple Interferences from the Same Source. *IEEE Transactions on Vehicular Technology*, *69*(7), 7583-7595. [9093218]. https://doi.org/10.1109/TVT.2020.2994332

Inside-Out Precoding to Manage Multiple Interferences From the Same Source

Zhao Li, *Member, IEEE*, Yujiao Bai, Kang G. Shin, *Life Fellow, IEEE*, Zheng Yan, *Senior Member, IEEE*, and Hui Li, *Member, IEEE*

***Abstract*—With the continually increasing demand for higher data rate and link density as well as better network coverage, wireless networks, including 5G-enabled vehicular communication network (VCN), will be designed/deployed to cover more overlapping areas, experiencing more severe interferences. As a result, interference becomes a key impediment to the improvement of network performance, thus requiring a thorough investigation. There have been numerous interference management (IM) methods, of which interference alignment (IA) has been receiving significant attention in recent years. IA compresses the dimension of interference subspace by confining multiple interfering signals into a finite subspace, so that the desired signal subspace may be maximized. However, when IA is applied to the situation where multiple interferences are from the same source, the interference subspace cannot be compressed due to the fact that if these interfering components are aligned in the same direction at their unintended receiver (Rx), they will become indistinguishable at their desired Rx. To solve this problem, we propose *Inside-Out Precoding* (IOP). With IOP, multiple data streams that may cause interference to the other Rx are at first pre-processed at the interfering transmitter (Tx), by employing an *inner-precoder* which makes the streams spatially separable, and then, by exploiting interactions among wireless signals, multiple interfering components are treated as an effective interference to which an *outer-precoder* is applied, so that multiple interferences can be compressed into one dimension at the interfered Rx while making them distinguishable at their desired Rx. We present two IOP realizations — *forward IOP* (F-IOP) and *backward IOP* (B-IOP) — and propose a protocol to realize the synchronization of processing parameters at the interfering Tx and its intended Rx so that the Rx can adapt itself to the precoding strategy employed at the Tx side. Our in-depth analysis and simulation results have shown that the proposed IOP can effectively manage multiple interferences from the same source while guaranteeing the performance of transmission from the interfering Tx to its intended Rx.**

***Index Terms*—Mobile communication, interference management, signal processing, interference alignment, precoding.**

Manuscript received December 16, 2019; revised March 16, 2020; accepted May 10, 2020. Date of publication May 14, 2020; date of current version July 16, 2020. This work was supported in part by the 111 Project under Grant B16037, in part by NSFC under Grant 61672410, and in part by the U.S. National Science Foundation under Grant 1317411. The review of this article was coordinated by Dr. C. Yuen. *(Corresponding author: Zhao Li.)*

Zhao Li, Zheng Yan, and Hui Li are with the School of Cyber Engineering, Xidian University, Xi'an, Shaanxi 710126, China (e-mail: zli@xidian.edu.cn; zyan@xidian.edu.cn; lihui@mail.xidian.edu.cn).

Yujiao Bai is with the School of Telecommunications Engineering, Xidian University, Xi'an, Shaanxi 710071, China (e-mail: yjbai1990@gmail.com).

Kang G. Shin is with the Department of Electrical Engineering and Computer Science, the University of Michigan, Ann Arbor, MI 48109-2121 USA (e-mail: kgshin@umich.edu).

Digital Object Identifier 10.1109/TVT.2020.2994332

I. Introduction

THE 5 G network is expected to have many salient features [1], such as ultra-high data rate, ultra-dense connectivity, ultra-low latency, etc. In 5 G, vehicular communication network (VCN) is one of the core application. The soaring number of connected cars with Internet access, along with the emerging vehicular mobile data services will altogether impose stringent requirements toward its enabling technology solutions [2]. Recently, vehicle-to-everything (V2X) has been proposed as a promising concept enabling diverse vehicular communication modes including vehicle-to-vehicle (V2V), vehicle-to-pedestrian (V2P), vehicle-to-infrastructure (V2I), and etc [3]. In future vehicular networks, various types of V2X communications co-exist and may share the same wireless medium for data transmissions, hence incurring complicated interference situation. Moreover, a vehicular network with road side units (RSUs) provides an efficient way to connect vehicles even on the move [4], however, full network coverage implies that overlapping among adjacent RSUs becomes inevitable.

While searching for new technologies to meet the continually increasing demands for various wireless applications in 5G-enabled VCN, *interference management* (IM) has become key to the improvement of network performance [5] and thus deserves a thorough investigation. For example, the authors of [6] studied the deployment of device-to-device (D2D)-enabled wireless networks with unmanned aerial vehicles (UAVs) in remote, rural, and disaster affected areas where cellular infrastructures are unavailable or inadequate. They argued that in such areas the allocation of radio channels to the UAV nodes and user terminals is challenging due to the number of orthogonal channels is limited and using overlapping channels in adjacent nodes leads to severe interference. Therefore, a distributed anti-coordination game based partially overlapping channel (AC-POCA) assignment algorithm was proposed to solve the above problem. In [7], deep learning was employed in the design of traffic load and congestion prediction and intelligent channel assignment algorithms, so that interference can be properly controlled while improving the network performance. The authors of [8] proposed a joint Tx and Rx design to combat inter-symbol interference (ISI) in frequency selective fading channel based on an approximate maximum likelihood decision feedback equalizer. The authors of [9] suggested that machine learning (ML) can be a powerful tool for channel assignment and interference management in 6 G networks.

The existing IM methods can be grouped in two types. The first type is featured as the interfered receiver (Rx) or/and its associated transmitter (Tx) side implementation, including zero-forcing (ZF) reception, interference neutralization (IN) [10], [11], interference steering (IS) [12], etc. The second type is characterized by the interfering Tx side implementation, such as zero-forcing beamforming (ZFBF) [13] and interference alignment (IA)[1] [16]–[22].

Of these methods, IN and IS have been under development in recent years [10]–[12]. IN strives to properly combine signals arriving through various paths in such a way that the interfering signals are canceled while the desired signals are preserved at the Rx [10], [11]. Although IN can mitigate interference, the power overhead of generating neutralizing signal(s) degrades the system performance as well [11]. Under IS, a steering signal is generated to modify the propagation of interference, so that the original interference is steered in the orthogonal direction of the desired transmission at the interfered Rx. Compared to IN, IS focuses on the cancellation of the effective part of interference, thus becoming more power-efficient [12], but an additional spatial DoF is required to place the steered interference. In [12], IS was proposed in Internet-of-Things (IoT) to address the interference problem. It has been demonstrated that IS can substantially improve network spectral efficiency (SE) over existing IM schemes.

However, as for the realization of IN and IS, the interfered Tx which is associated with the interfered Rx needs to know the interference information including both the channel state information (CSI) from the interfering Tx to the interfered Rx and the data information carried in the interference. Such information requires high-level cooperation between the interfering and interfered Txs, incurring the algorithm complexity and the signaling overhead. Besides, both IN and IS are interfered-Tx-based IM, and it is, in practice, unfair to make the interfered transmission pair responsible for all of IM, since IM will incur some "cost" such as power [10], [11] and DoF [12] consumption which leads to communication performance loss, especially when the interfered transmission pair has the same or higher priority than the interfering Tx. Therefore, the interferer is amenable to more or less IM responsibility.

As for the interfering Tx side IM, [13] has shown that ZFBF strategy used in multiple-input multiple-output (MIMO) broadcast channel (BC), while generally suboptimal, can achieve the same asymptotic sum capacity as that of dirty paper coding (DPC), as the number of users goes to infinity. However, for ZFBF, the DoF requirement is determined by the total number of desired signals and interference, i.e., each interfering signal component consumes one DoF [12]. Compared to ZFBF, IA has been shown to be able to achieve the information-theoretic maximum DoFs in some interference networks [16], [17], and is thus regarded as a promising IM method. With IA, interference is adjusted at the interfering source so that multiple interfering signals are mapped into a finite subspace, i.e., the overall interference space at the unintended destination/Rx is minimized, while the desired signal(s) may be sent through a subspace without attenuation [18]. IA has been under extensive study and development since it was systematized in [16]. Existing studies have shown that IA can be applied to various communication environments, such as cellular networks [19], [20] and wireless relays [21], [23]. In [19], an IA-based coordinated beamforming was proposed to improve the downlink performance of multiple cell-edge users in multi-user MIMO systems. In [20], an IA-based uplink IM for two-tier cellular systems was proposed. [21] proposed a pair-aware IA to achieve interference alignment in a multi-user two-way relay network. [23] investigated the DoF for the fully-connected M-user interference channel (IC) in static environments with the help of a MIMO relay. The relay stores the received signal during the first time-slot and sends a linearly-transformed version over the next time-slot. Using this scheme, it has been shown that IA can be achieved with much less complexity. In addition to designing IA individually/separately, combining IA with other methods generates many new methods and makes further performance improvements. [24] presented interference alignment and cancellation (IAC) for decoding concurrent sender-receiver pairs in MIMO networks and showed that the combination applies to scenarios where neither interference alignment nor cancellation applies alone. In [25], interference alignment and neutralization (IAN) based coordinated multi-point (CoMP) was proposed. Effective interference cancellation and suppression can be achieved by exploiting limited and flexible collaboration at the base station (BS) side.

Although IA has been regarded as a promising method and under development for many years, it has been shown that the feasibility of IA is highly dependent on system parameters, such as the numbers of Txs and Rxs, configuration of transmit/receive antennas, and so on [18]. Moreover, when multiple interferences are from one identical Tx, traditional IA may become inapplicable [5]. That is, if the interfering signals originated from the same source and intended to the same Rx are aligned in one direction at an unintended Rx, they will also overlap with each other at their common destination, thus becoming indistinguishable.

To remedy this deficiency of IA, we propose *Inside-Out Precoding* (IOP) to manage multiple interfering signals from the same source. First, we argue that the goal of IM is limiting the effect of interference rather than managing individual interferences. Following this argument, the dimension of interference to be managed is reduced to 1 regardless of the number of interference signals. Then, by employing inner and outer precoders, multiple interfering signals are aligned in the orthogonal subspace with respect to the interfered transmission; these pre-processed signals can still be distinguished at their intended Rx. The proposed IOP is implemented at the interfering Tx and consumes only one DoF at the interfered Rx, while the interfered transmission pair need not any modification, thus facilitating the deployment of IOP.

The contributions of this paper are three-fold:

- A new finding that IM is limiting the effect of interference perceived by the interfered Rx, rather than managing

[1] Since many practical systems are equipped with multiple antennas which has been known to greatly increase the degrees of freedom (DoFs) of communication systems [14], in this work we consider the realization of IA in multi-antenna systems without requiring symbol extensions over very large number of time-frequency dimensions [15].

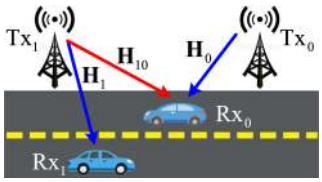

Fig. 1. System model.

individual interference. By exploiting inter-relationship of transmitted symbols carried by multiple interfering signals, the dimension of interference to be managed is reduced to 1 regardless of the number of interferences.

- Proposal of *Inside-Out Precoding* (IOP) to manage multiple interferences from the same source. An inner-precoder is employed to distinguish multiple signals at their intended Rx, while an outer-precoder is designed to align the overall interfering effect of these signals in the orthogonal subspace with respect to the unintended Rx's desired transmission.
- Development of two IOP implementations — forward IOP (F-IOP) and backward IOP (B-IOP) — as well as a protocol to achieve the synchronization of processing parameters at the interfering Tx and its intended Rx so that the Rx can adapt itself to the precoding strategy employed by the Tx. With the proposed schemes, the interferer's transmission performance can be well guaranteed while avoiding interference to the intended Rx.

The rest of this paper is organized as follows. Section II describes the system model, while Section III details the forward IOP scheme. Section IV presents the backward IOP and Section V provides a protocol to facilitate the reception of the interfering Tx–Rx pair. Section VI evaluates the performance of the proposed schemes. Finally, Section VII concludes the paper.

In the rest of this paper, we will use the following notations. The set of complex numbers is denoted as $\mathbb{C}$, while vectors and matrices are represented by bold lower-case and upper-case letters. Let $\mathbf{X}^T$, $\mathbf{X}^H$ and $\mathbf{X}^{-1}$ denote the transpose, Hermitian, and inverse of matrix $\mathbf{X}$, respectively. $\|\cdot\|$ and $|\cdot|$ indicate the Euclidean norm and the absolute value. $\mathbb{E}(\cdot)$ denotes statistical expectation and $\langle \mathbf{a}, \mathbf{b} \rangle$ represents the inner product of two vectors.

II. System Model

We consider the Z-interference channel (ZIC) [26] as shown in Fig. 1 with two communication pairs, one Rx (i.e., vehicle) of which suffers interference from an unintended Tx (i.e., RSU or other infrastructures) while the other Rx is free from interference. Tx_i and Rx_i (transmitter/receiver indexed by $i = 0, 1$) are equipped with N_{T_i} and N_{R_i} antennas, respectively. The transmit power of Tx_i is P_T. Without loss of generality, we let transmission from Tx_1 to Rx_1 interfere with that from Tx_0 to Rx_0, while Rx_1 is free from interference [27]. The data-transmission channel matrix from Tx_i to Rx_i is denoted as $\mathbf{H}_i \in \mathbb{C}^{N_{R_i} \times N_{T_i}}$, and the interference channel matrix from Tx_1 to Rx_0 is represented by $\mathbf{H}_{10} \in \mathbb{C}^{N_{R_0} \times N_{T_1}}$. We use a spatially uncorrelated Rayleigh flat fading channel model to model the elements of these two matrices as independent and identically distributed zero-mean unit-variance complex Gaussian random variables. We assume that all users experience block fading, i.e., channel parameters remain constant within a block consisting of several successive time slots and vary randomly over successive blocks. Each user can accurately estimate CSI with respect to its intended and unintended Txs and feed it back to the associated Tx via a low-rate, error-free link. We assume reliable links for the delivery of CSI and signaling. The delivery delay is negligible compared to the time scale on which the channel state varies.

We employ $\mathbf{X}_0 = [x_0^{(1)} \cdots x_0^{(m)} \cdots x_0^{(M)}]^T$ and $\mathbf{X}_1 = [x_1^{(1)} \cdots x_1^{(k)} \cdots x_1^{(K)}]^T$ to denote the transmit data vectors from Tx_0 and Tx_1 where $x_0^{(m)}$ and $x_1^{(k)}$ represent the m^{th} and k^{th} symbols in $\mathbf{X}_0$ and $\mathbf{X}_1$, respectively. $\mathbb{E}(\|x_0^{(m)}\|^2) = P_T/M$ and $\mathbb{E}(\|x_1^{(k)}\|^2) = P_T/K$ hold. We assume $M + K > N_{R_0}$ where ZF reception and IA are not applicable due to the lack of DoFs at Rx_0. For clarity of exposition, our design begins with $N_{T_1} \geq K > 1$, $N_{R_1} \geq K > 1$, and $N_{T_0} \geq M = 1$, and $N_{R_0} = M + 1$, i.e., Tx_1 employs *spatial multiplexing* (SM) to transmit $K > 1$ data streams to Rx_1 causing multiple interferences to Rx_0, while Tx_0 adopts *beamforming* (BF) to send a single ($M = 1$) data stream to Rx_0.

III. Design of Inside-Out Precoding

This section elaborates on the design of IOP. We first state the goal of IM for managing the effect of interference on the interfered Rx, not individual interferences. We then detail the design of inner and outer precoders consisting IOP.

A. Management of Interference Effect

Based on the system model given in Fig. 1, the received signals at Rx_0 and Rx_1 can be expressed by Eqs. (1) and (2) as:

$$\mathbf{y}_0 = \mathbf{H}_0 \mathbf{p}_0^{(1)} x_0^{(1)} + \mathbf{H}_{10} \sum_{k=1}^{K} \mathbf{p}_1^{(k)} x_1^{(k)} + \mathbf{n}_0, \tag{1}$$

$$\mathbf{y}_1 = \mathbf{H}_1 \sum_{k=1}^{K} \mathbf{p}_1^{(k)} x_1^{(k)} + \mathbf{n}_1. \tag{2}$$

The first terms on the right-hand-side (RHS) of the above equations represent the desired signals for Rx_0 and Rx_1, respectively. The second term on the RHS of Eq. (1) denotes the interference from Tx_1. $\mathbf{p}_0^{(1)} \in \mathbb{C}^{N_{T_0} \times 1}$ and $\mathbf{p}_1^{(k)} \in \mathbb{C}^{N_{T_1} \times 1}$ where $k = 1, 2, \ldots, K$, are the precoding vectors for data $x_0^{(1)}$ and $x_1^{(k)}$ at Tx_0 and Tx_1, respectively. For simplicity, we define $\mathbf{P}_1 = [\mathbf{p}_1^{(1)} \, \mathbf{p}_1^{(2)} \cdots \mathbf{p}_1^{(K)}]$. $\mathbf{n}_i \in \mathbb{C}^{N_{R_i} \times 1}$ $(i = 0, 1)$ is additive white Gaussian noise (AWGN) vector whose elements have zero-mean and variance σ_n^2. $\mathbb{E}(\mathbf{n}_i \mathbf{n}_i^H) = \mathbf{I}_{N_{R_i}}$ holds, where $\mathbf{I}_{N_{R_i}}$ is an $N_{R_i} \times N_{R_i}$ identity matrix.

Since we set $N_{T_i} > 1, N_{R_0} = M + 1, K > 1$ and $M = 1$, the lack of DoF at Rx_0 makes ZF and IA inapplicable. Especially for IA, if we adjust K signals at Tx_1 so as to align them in the same direction at Rx_0, these pre-processed signals will become indistinguishable at their intended receiver, Rx_1. That

is, transmission from Tx_1 to Rx_1 is completely sacrificed for the IM.

Based on the above analysis, insufficient DoF at the interfered Rx is a key limitation for the applicability of IM. We may either increase the supply of DoF at Rx or reduce the DoF requirement of IM. However, the former will impose hardware and complexity burdens on the Rx, especially for the downlink transmission, but mobile stations always have rigid restrictions on the equipment size, cost, etc. So, we present a novel idea of IM — managing the overall effect of interferences instead of managing them individually.

To elaborate the above idea, we explore the inter-relationship of transmitted symbols carried by K interfering signals. For clarity of exposition, we assume all the interfering signals are generated using the same modulation scheme. Let $S = \{s_1, s_2, \ldots, s_L\}$ denote the symbol set. The size of S is $\text{card}(S) = L$ where $\text{card}(\cdot)$ represents the cardinality of set S, and L indicates the modulation order. Since each element in S can be represented by its amplitude and phase, we take an arbitrary symbol in S, say, s_l ($l \in \{1, 2, \ldots, L\}$), as an example. s_l can be expressed as $s_l = a_l e^{j\theta_l}$ where a_l and θ_l denote s_l's amplitude and phase, respectively.

Let us define the transmitted symbol $x_1^{(\hat{k})} \in S$, i.e., $x_1^{(\hat{k})} = a_{\hat{l}} e^{j\theta_{\hat{l}}}$. Without loss of generality, we take $x_1^{(\hat{k})}$ as the referential symbol, then all the other symbols $x_1^{(k)}$ ($k \in \{1, 2, \ldots, K\}, k \neq \hat{k}$) can be expressed in terms of $x_1^{(\hat{k})}$ as:

$$x_1^{(k)} = \frac{a_l}{a_{\hat{l}}} e^{j(\theta_l - \theta_{\hat{l}})} x_1^{(\hat{k})} = b_{k\hat{k}} x_1^{(\hat{k})} \tag{3}$$

where $b_{k\hat{k}} = \frac{a_l}{a_{\hat{l}}} e^{j(\theta_l - \theta_{\hat{l}})}$ ($\hat{l}, l \in \{1, 2, \ldots, L\}$ and $\hat{l} \neq l$). Note that when $\hat{l} = l$, we have $b_{k\hat{k}} = 1$. Then the interference term in Eq. (1) becomes:

$$\mathbf{i}^{(\Sigma)} = \mathbf{H}_{10} \sum_{k=1}^{K} \mathbf{p}_1^{(k)} x_1^{(k)} = \mathbf{H}_{10} \sum_{k=1}^{K} \mathbf{p}_1^{(k)} b_{k\hat{k}} x_1^{(\hat{k})}. \tag{4}$$

By defining $\mathbf{p}_e = \sum_{k=1}^{K} \mathbf{p}_1^{(k)} b_{k\hat{k}}$ and $x_e = x_1^{(\hat{k})}$, and substituting $\mathbf{p}_e$ and x_e into Eq. (1), we can have:

$$\mathbf{y}_0 = \mathbf{H}_0 \mathbf{p}_0^{(1)} x_0^{(1)} + \mathbf{H}_{10} \mathbf{p}_e x_e + \mathbf{n}_0. \tag{5}$$

From Eq. (5) one can see that by exploiting the interactions among multiple signals, the dimension of interference to be managed is reduced to 1 regardless of the number of interfering components. This is consistent with the intuitive that in the design of IM, one should focus on the influence of interference on the interfered Rx rather than individual interferences. However, existing IM strategies focus on how to manage individual interferences, hence incurring more IM overhead, implementation complexity, and stricter application constraints in multi-interference scenarios.

B. Design of Inner-Precoder

We employ $\mathbf{P}_1 = [\mathbf{p}_1^{(1)}\, \mathbf{p}_1^{(2)}\, \cdots\, \mathbf{p}_1^{(K)}]$ where $K \leq \min(N_{T_1}, N_{R_1})$, as the inner-precoder for $\mathbf{X}_1$. The design objective of $\mathbf{P}_1$ is to distinguish various data transmissions at Rx_1. There have been numerous precoding schemes to achieve this goal. For simplicity, we employ the precoding based on singular value decomposition (SVD), a commonly used pre-processing method in MIMO communications.

Applying SVD to $\mathbf{H}_1$, we have $\mathbf{H}_1 = \mathbf{U}_1 \mathbf{\Sigma}_1 \mathbf{V}_1^H$ where $\mathbf{U}_1 = [\mathbf{u}_1^{(1)}\, \mathbf{u}_1^{(2)}\, \cdots\, \mathbf{u}_1^{(N_{R_1})}]$ and $\mathbf{V}_1 = [\mathbf{v}_1^{(1)}\, \mathbf{v}_1^{(2)}\, \cdots\, \mathbf{v}_1^{(N_{T_1})}]$ are the right and left singular matrices. $\mathbf{\Sigma}_1$ is an $N_{R_1} \times N_{T_1}$ diagonal matrix whose non-zero main diagonal elements, a.k.a., non-zero singular values of $\mathbf{H}_1$, denote the amplitude gain of spatial sub-channels characterized by $\mathbf{v}_1^{(k)}$ and $\mathbf{u}_1^{(k)}$ where $k = 1, 2, \ldots, \min(N_{T_1}, N_{R_1})$. We adopt $\mathbf{P}_1 = \mathbf{V}_1$, i.e., $\mathbf{p}_1^{(k)} = \mathbf{v}_1^{(k)}$, as the inner precoder.

C. Design of Outer-Precoder

We now detail the design of outer-precoder, denoted by $\mathbf{G}_e \in \mathbb{C}^{N_{T_1} \times N_{T_1}}$. By applying $\mathbf{G}_e$ to the equivalent interference $\mathbf{i}^{(\Sigma)}$ given in Eq. (4), we must achieve two goals: 1) the effective interference $\mathbf{i}^{(\Sigma)}$ is adjusted to the orthogonal subspace with respect to the transmission from Tx_0 to Rx_0, and 2) multiple signals sent from Tx_1 are distinguishable at their intended receiver Rx_1.

By employing inner and outer precoders, i.e., $\mathbf{P}_1$ and $\mathbf{G}_e$, we can rewrite Eqs. (5) and (2) as:

$$\mathbf{y}_0 = \mathbf{H}_0 \mathbf{p}_0^{(1)} x_0^{(1)} + \mathbf{H}_{10} \mathbf{G}_e \mathbf{p}_e x_e + \mathbf{n}_0, \tag{6}$$

$$\mathbf{y}_1 = \mathbf{H}_1 \mathbf{G}_e \mathbf{p}_e x_e + \mathbf{n}_1 \tag{7}$$

where $\mathbf{p}_e = \sum_{k=1}^{K} \mathbf{p}_1^{(k)} b_{k\hat{k}}$ and $b_{k\hat{k}} = x_1^{(k)} / x_1^{(\hat{k})}$. $x_e = x_1^{(\hat{k})}$ and $x_1^{(\hat{k})}$ represents for the referential symbol.

$\mathbf{G}_e$ should satisfy the following two conditions,

$$\begin{cases} \mathbf{H}_0 \mathbf{p}_0^{(1)} \perp \mathbf{H}_{10} \mathbf{G}_e \mathbf{p}_e \\ \left| \langle \mathbf{e}_{\mathbf{H}_1 \mathbf{G}_e \mathbf{p}_1^{(l)}}, \mathbf{e}_{\mathbf{H}_1 \mathbf{G}_e \mathbf{p}_1^{(k)}} \rangle \right| < \beta \end{cases} \tag{8}$$

where $l, k \in \{1, 2, \ldots, K\}$ and $l \neq k$. $\mathbf{e}_{\mathbf{H}_1 \mathbf{G}_e \mathbf{p}_1^{(l)}} = \frac{\mathbf{H}_1 \mathbf{G}_e \mathbf{p}_1^{(l)}}{\|\mathbf{H}_1 \mathbf{G}_e \mathbf{p}_1^{(l)}\|}$ and $\mathbf{e}_{\mathbf{H}_1 \mathbf{G}_e \mathbf{p}_1^{(k)}} = \frac{\mathbf{H}_1 \mathbf{G}_e \mathbf{p}_1^{(k)}}{\|\mathbf{H}_1 \mathbf{G}_e \mathbf{p}_1^{(k)}\|}$ indicate the signatures of signals carrying $x_1^{(l)}$ and $x_1^{(k)}$, respectively. $\beta \in (0, 1)$. The smaller β is, unit vectors $\mathbf{e}_{\mathbf{H}_1 \mathbf{G}_e \mathbf{p}_1^{(l)}}$ and $\mathbf{e}_{\mathbf{H}_1 \mathbf{G}_e \mathbf{p}_1^{(k)}}$ are less correlated.

The first equation of Eq. (8) is employed to design $\mathbf{G}_e$ so that the equivalent interference $\mathbf{i}^{(\Sigma)} = \mathbf{H}_{10} \mathbf{G}_e \mathbf{p}_e$ can be adjusted to be orthogonal to the desired signal at Rx_0; while the second equation is used to guarantee the signal components causing interference to Rx_0 are distinguishable at their intended receiver, Rx_1. The first equation of Eq. (8) can be simplified as:

$$\mathbf{H}_{10} \mathbf{G}_e \mathbf{p}_e = \alpha \mathbf{d}_\perp \tag{9}$$

where $\mathbf{d}_\perp$ is a unit vector denoting the orthogonal direction with respect to the signature of the transmission from Tx_0 to Rx_0, and α is a complex coefficient indicating that the vectors on both sides of the equation are in the same direction but scalable modules. It should be noticed that the design of IOP can be easily extended to the case of $M > 1$. In this situation, we only need to substitute $\mathbf{H}_0 \mathbf{p}_0^{(1)}$ in the first equation of Eq. (8)

with the expression of the subspace spanned by the M desired transmissions.

Next, we detail the calculation of $\mathbf{G}_e$. By left-multiplying by $\mathbf{H}_{10}^{-1}$ at both sides of Eq. (9) and employing $\mathbf{b} = \mathbf{H}_{10}^{-1}\mathbf{d}_\perp = [b^{(1)}\, b^{(2)}\, \cdots\, b^{(N_{T_1})}]^T$, Eq. (10) can be obtained as:

$$\mathbf{G}_e\mathbf{p}_e = \alpha\mathbf{b} \tag{10}$$

where $\mathbf{G}_e = \begin{bmatrix} g_e^{(11)} & g_e^{(12)} & \cdots & g_e^{(1N_{T_1})} \\ g_e^{(21)} & g_e^{(22)} & \cdots & g_e^{(2N_{T_1})} \\ \vdots & \vdots & \ddots & \vdots \\ g_e^{(N_{T_1}1)} & g_e^{(N_{T_1}2)} & \cdots & g_e^{(N_{T_1}N_{T_1})} \end{bmatrix}$ and $\mathbf{p}_e = [p_e^{(1)}\, p_e^{(2)}\, \cdots\, p_e^{(N_{T_1})}]^T$.

Note that if $\mathbf{H}_{10}$ is not square matrix, $\mathbf{H}_{10}^{-1}$ should be replaced by $\mathbf{H}_{10}$'s pseudo inverse $\mathbf{H}_{10}^{\dagger} = (\mathbf{H}_{10}^H\mathbf{H}_{10})^{-1}\mathbf{H}_{10}^H$. That is, IOP is applicable under $N_{T_1} \le N_{R_0}$. By applying elementary row operations, Eq. (10) can be rewritten as:

$$[p_e^{(1)}\mathbf{I}_{N_{T_1}}\, \cdots\, p_e^{(N_{T_1})}\mathbf{I}_{N_{T_1}}][(\mathbf{g}_e^{(1)})^T\, \cdots\, (\mathbf{g}_e^{(N_{T_1})})^T]^T = \alpha\mathbf{b} \tag{11}$$

where $[p_e^{(1)}\mathbf{I}_{N_{T_1}}\, \cdots\, p_e^{(N_{T_1})}\mathbf{I}_{N_{T_1}}]$ and $[(\mathbf{g}_e^{(1)})^T\, \cdots\, (\mathbf{g}_e^{(N_{T_1})})^T]^T$ are coefficient matrix and solution vector of Eq. (11), respectively. $\mathbf{I}_{N_{T_1}}$ is an $N_{T_1} \times N_{T_1}$ identity matrix, and $\mathbf{g}_e^{(i)}$ where $i = 1, 2, \ldots, N_{T_1}$ denotes the i^{th} column of $\mathbf{G}_e$.

Eq. (11) is a complex matrix equation. Its solution vector can be calculated based on Theorem 1.

Theorem 1 ([28]): For a complex non-homogeneous matrix equation $\mathbf{Ax} = \mathbf{b}$ where $\mathbf{A} \in \mathbb{C}^{m\times n}$ and $\mathbf{b} \in \mathbb{C}^{m\times 1}$. The necessary and sufficient condition that the solution for $\mathbf{x}$ exists is $\mathbf{AA}^{(1)}\mathbf{b} = \mathbf{b}$ holds. In such a case, $\mathbf{x} = \mathbf{A}^{(1)}\mathbf{b} + [\mathbf{I} - \mathbf{A}^{(1)}\mathbf{A}]\mathbf{k}$ ($\mathbf{k} \in \mathbb{C}^{n\times 1}$) where $\mathbf{A}^{(1)}$ satisfies $\mathbf{AA}^{(1)}\mathbf{A} = \mathbf{A}$.

For clarity of exposition, we take $N_{T_1} = N_{R_1} = N_{R_0} = K = 2$ as an example to solve Eq. (11). Then, we can get:

$$\mathbf{G}_e = \begin{bmatrix} \dfrac{\alpha b^{(1)} - k^{(3)}p_e^{(2)}}{p_e^{(1)}} & k^{(3)} \\ \dfrac{\alpha b^{(2)} - k^{(4)}p_e^{(2)}}{p_e^{(1)}} & k^{(4)} \end{bmatrix} \tag{12}$$

where $\mathbf{k} = [k^{(1)}\, k^{(2)}\, k^{(3)}\, k^{(4)}]^T$. Since $k^{(1)}$ and $k^{(2)}$ are eliminated as Eq. (12) shows, $\mathbf{G}_e$ is independent of these two complex coefficients when $\mathbf{G}_e$ is derived. Therefore, we can write $\mathbf{k} = [-\ -\ k^{(3)}\, k^{(4)}]^T$ or $\mathbf{k} = [k^{(3)}\, k^{(4)}]^T$ for short.

Similarly, we can have $\mathbf{G}_e$ under $N_{T_1} = 3, 4, \ldots$ as well. For simplicity, we do not show the results here. Then, by using mathematical induction, we can obtain a general solution for $\mathbf{G}_e$ given by Eq. (13), shown at the bottom of this page.

Based on the above discussion, $\mathbf{G}_e$ is dependent on the selection of $\mathbf{k}$. It should be noticed that in Eq. (13) $\mathbf{k} = [k^{(1)}\, \cdots\, k^{(N_{T_1})}\, k^{(N_{T_1}+1)}\, \cdots\, k^{(N_{T_1}^2)}]^T$. However, as $k^{(1)}$, $k^{(2)}$, $\ldots$, and $k^{(N_{T_1})}$ are eliminated in the derivation of $\mathbf{G}_e$, $\mathbf{k}$ can be written as $\mathbf{k} = [-\ \cdots\ -\ k^{(N_{T_1}+1)}\, \cdots\, k^{(N_{T_1}^2)}]^T$ or $\mathbf{k} = [k^{(N_{T_1}+1)}\, \cdots\, k^{(N_{T_1}^2)}]^T$ for short. In what follows, we will elaborate on the selection of proper solutions for $\mathbf{G}_e$ by taking the second equation of Eq. (8) into account. Before delving into details, we first provide two claims.

Claim 1: The design of $\mathbf{G}_e$ should satisfy $\text{rank}(\mathbf{G}_e) = K$ where K is the number of desired signals from Tx_1 to Rx_1. Otherwise, if $\text{rank}(\mathbf{G}_e) < K$, Rx_1 will not be able to distinguish K signal components.

See the proof of Claim 1 in Appendix A.

Taking $N_{T_1} = N_{R_1} = N_{R_0} = K = 2$ as an example, when we set $k^{(3)} = k^{(4)} = 0$, $\text{rank}(\mathbf{G}_e) = 1$ is obtained. Then, $\text{rank}(\mathbf{H}_1\mathbf{G}_e\mathbf{P}_1) \le \text{rank}(\mathbf{G}_e) = 1$ holds where $\text{rank}(\mathbf{P}_1) = K$. That is, the spatial signatures of the signals carrying $x_1^{(1)}$ and $x_1^{(2)}$ are linearly correlated (overlapping with each other in this case), and hence they cannot be de-correlated at their intended receiver. Given $1 < \text{rank}(\mathbf{G}_e) < K$, at most $\text{rank}(\mathbf{G}_e)$ data streams can be de-correlated at Rx_1.

Claim 2: The design of $\mathbf{G}_e$ should satisfy that $|\langle \mathbf{e}_{\mathbf{H}_1\mathbf{G}_e\mathbf{p}_1^{(l)}}, \mathbf{e}_{\mathbf{H}_1\mathbf{G}_e\mathbf{p}_1^{(k)}} \rangle|$ is as close to 0 as possible where $l, k \in \{1, 2, \ldots, K\}$ and $l \ne k$. Otherwise, if $|\langle \mathbf{e}_{\mathbf{H}_1\mathbf{G}_e\mathbf{p}_1^{(l)}}, \mathbf{e}_{\mathbf{H}_1\mathbf{G}_e\mathbf{p}_1^{(k)}} \rangle| \approx 1$, severe desired signal's power loss will be incurred when eliminating interference from the transmission of $x_1^{(l)}$ (or $x_1^{(k)}$) to that of the other, i.e., $x_1^{(k)}$ (or $x_1^{(l)}$).

See the proof of Claim 2 in Appendix B.

Based on the above discussion, upon obtaining a particular solution of $\mathbf{G}_e$ that satisfies the first equation in Eq. (8), we should verify its validity in terms of Claims 1 and 2, so that good transmission performance of Tx_1–Rx_1 pair can be guaranteed.

In summary, we provide an algorithm below to show the processing of the proposed IOP.

Fig. 2 plots spatial spectrums of various signals at Rx_0 and Rx_1 to show the feasibility of IOP. We set $N_{T_1} = N_{R_1} = N_{R_0} = 2$ and let Tx_1, the interfering transmitter, send $K = 2$ data streams to Rx_1, causing interference to Rx_0. Tx_1 employs BPSK modulation. The inner precoder $\mathbf{P}_1 = \mathbf{V}_1$ where $\mathbf{V}_1$ is the right singular matrix of $\mathbf{H}_1$. The center frequency of input signal is $f_0 = 2.4$ GHz, the antenna-element spacing is a half of the signal wavelength, and the signal to noise ratio (SNR) of each signal

$$\mathbf{G}_e = \begin{bmatrix} \dfrac{\alpha b^{(1)} - \sum_{i=1}^{N_{T_1}-1} k^{(iN_{T_1}+1)} p_e^{(i+1)}}{p_e^{(1)}} & k^{(N_{T_1}+1)} & k^{(2N_{T_1}+1)} & \cdots & k^{(N_{T_1}-1)N_{T_1}+1} \\ \dfrac{\alpha b^{(2)} - \sum_{i=1}^{N_{T_1}-1} k^{(iN_{T_1}+2)} p_e^{(i+1)}}{p_e^{(1)}} & k^{(N_{T_1}+2)} & k^{(2N_{T_1}+2)} & \cdots & k^{(N_{T_1}-1)N_{T_1}+2} \\ \vdots & \vdots & \vdots & \ddots & \vdots \\ \dfrac{\alpha b^{(N_{T_1})} - \sum_{i=1}^{N_{T_1}-1} k^{(iN_{T_1}+N_{T_1})} p_e^{(i+1)}}{p_e^{(1)}} & k^{(N_{T_1}+N_{T_1})} & k^{(2N_{T_1}+N_{T_1})} & \cdots & k^{(N_{T_1}-1)N_{T_1}+N_{T_1}} \end{bmatrix} \tag{13}$$

Algortim 1:

1: Rx_0 estimates $\mathbf{H}_0$ and $\mathbf{H}_{10}$, Rx_1 estimates $\mathbf{H}_1$. Then, Rx_0 and Rx_1 feed back CSI to their associated Txs, respectively. Tx_0 shares $\mathbf{H}_0$ and $\mathbf{H}_{10}$ with Tx_1.
2: Tx_1 determines inner precoder $\mathbf{P}_1$ (e.g., in terms of certain precoding schemes such as SVD based pre-processing).
3: Tx_1 calculates $\mathbf{p}_e$ based on $\mathbf{P}_1$, and substitutes $\mathbf{p}_e$ into Eq. (13) to obtain general solution for $\mathbf{G}_e$ with unknown parameters α and $\mathbf{k}$.
4: Tx_1 randomly generates α and $\mathbf{k}$, and substitutes them into the general solution for $\mathbf{G}_e$ to obtain particular solution for $\mathbf{G}_e$.
5: **If** $\text{rank}(\mathbf{G}_e) = K$, execute Step 6;
Else return to Step 4.
6: **For** $l = 1$ to K **do**
For $k = 1$ to K **do**
If $l \neq k$, calculate $\rho_{lk} = |\langle \mathbf{e}_{\mathbf{H}_1\mathbf{G}_e\mathbf{p}_1^{(l)}}, \mathbf{e}_{\mathbf{H}_1\mathbf{G}_e\mathbf{p}_1^{(k)}} \rangle|$ at Tx_1;
If $\rho_{lk} \geq \beta$, break and return to Step 4;
Else;.
Else;.
End For
End For
Execute Step 7.
7: Tx_1 employs $\mathbf{P}_1$ and $\mathbf{G}_e$ to perform precoding for $\mathbf{X}_1$.

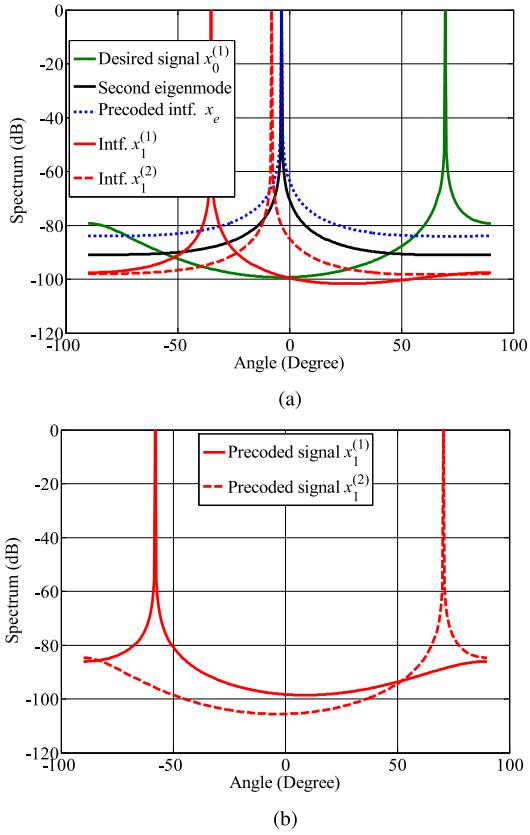

Fig. 2. Spatial spectrums of different signals. (a) Spatial spectrums at Rx_0. (b) Spatial spectrums at Rx_1.

is 20 dB. We first employ the MUSIC (MUltiple SIgnal Classification) algorithm to estimate DoA (Direction of Arrival) of each signal. Then, we reconstruct the spatial spectrum of signal components observed at the receiver. For ease of comparison, we also plot signal transmission via the second eigenmode of $\mathbf{H}_0$ which is orthogonal to the desired signal of Rx_0 occupying the principal eigenmode.

As Fig. 2(a) shows, the effect (carrying data x_e which can be either $x_1^{(1)}$ or $x_1^{(2)}$) of the two interfering components (carrying $x_1^{(1)}$ and $x_1^{(2)}$, respectively) is adjusted to the second eigenmode of $\mathbf{H}_0$ by applying IOP at Tx_1. That is, the pre-processed effect of the two interferences at Rx_0 is orthogonal to the desired transmission from Tx_0 to it. In Fig. 2(b), two precoded desired signals at Rx_1 are spatially distinguishable. Therefore, according to Fig. 2, the use of IOP satisfies the conditions given by Eqs. (8) and (9).

IV. Design of Backward IOP

From the design of outer-precoder given in Section III-C, one can see that if an inappropriate $\mathbf{k}$ is adopted (see in Eq. (13)), an infeasible $\mathbf{G}_e$ not satisfying Claim 1 or 2 may result. In such a case, we need to select another $\mathbf{k}$ and then verify the validity of the particular solution for $\mathbf{G}_e$ in terms of Claims 1 and 2. Moreover, in terms of the proof of Claim 2, when either $\varepsilon_1 \to 0$ or $\varepsilon_2 \to 0$, $\mathbf{H}_1\mathbf{G}_e\mathbf{p}_1^{(1)} \approx \mathbf{H}_1\mathbf{G}_e\mathbf{p}_1^{(2)}$ holds. In such a case, no matter what values $k^{(3)}$, $k^{(4)}$ and α are taken, signatures of the two precoded signals are close to each other, thus incurring severe desired signal's power loss while eliminating mutual interference. So, IOP is not suitable for such channel realizations.

In order to solve this problem, we propose a *Backward IOP* (B-IOP) realization in this section (we call the scheme presented in Section III-C the *Forward IOP* (F-IOP)). With B-IOP, Tx_1 first selects a matrix $\mathbf{C}_i$ (codeword indexed by i) from the codebook configured in it as the design target of the cascaded precoding matrix $\mathbf{G}_e\mathbf{P}_1$, where $\mathbf{G}_e$ and $\mathbf{P}_1$ satisfies the first equation in Eq. (8). In practice, the codeword can be chosen to match $\mathbf{H}_1$ as much as possible, so as to yield the maximum SE of the interfering Tx–Rx pair. Next, a general solution for $\mathbf{G}_e$ with unknown parameters α, $\mathbf{k}$ and $\mathbf{p}_e$ is obtained similarly to the derivation of Eq. (13). Finally, $\mathbf{G}_e$ and $\mathbf{P}_1$ are solved in terms of Eq. (15) as:

$$\mathbf{G}_e\mathbf{P}_1 = \mathbf{C}_i. \tag{14}$$

Then, we substitute Eq. (12) in (14) to get a new equation where $\mathbf{p}_e$ is still unknown. By solving such an equation with certain iterative algorithms [29], both $\mathbf{G}_e$ and $\mathbf{P}_1$ can be obtained.

Let's consider $N_{T_1} = N_{R_1} = N_{R_0} = K = 2$ as an example, to obtain $\mathbf{G}_e$ and $\mathbf{P}_1$ by using B-IOP. Then, we get Eq. (15) as:

$$\mathbf{G}_e\mathbf{P}_1 = \begin{bmatrix} \frac{\alpha b^{(1)} - k^{(3)} p_e^{(2)}}{p_e^{(1)}} & k^{(3)} \\ \frac{\alpha b^{(2)} - k^{(4)} p_e^{(2)}}{p_e^{(1)}} & k^{(4)} \end{bmatrix} \begin{bmatrix} p_1^{(11)} & p_1^{(12)} \\ p_1^{(21)} & p_1^{(22)} \end{bmatrix} = \mathbf{C}_i. \tag{15}$$

Let Tx_1 employ BPSK for data transmissions. Without loss of generality, we assume $x^{(1)}=1$ and $x_1^{(2)}=-1$, and $x^{(1)}$ is taken as the referential symbol. In Eq. (15), $b^{(1)}$ and $b^{(2)}$ are known parameters, determined by $\mathbf{H}_0$ and $\mathbf{H}_{10}$ whereas $p_1^{(11)}$, $p_1^{(12)}$, $p_1^{(21)}$, $p_1^{(22)}$, $p_e^{(1)}$ and $p_e^{(2)}$ are unknowns. Since $\mathbf{p}_1^{(1)}x_1^{(1)}+\mathbf{p}_1^{(2)}x_1^{(2)}=\mathbf{p}_1^{(1)}-\mathbf{p}_1^{(2)}=\mathbf{p}_e$ holds, we substitute $p_1^{(11)}=p_e^{(1)}+p_1^{(12)}$ and $p_1^{(21)}=p_e^{(2)}+p_1^{(22)}$ into Eq. (15), so that the number of unknowns is reduced to 4. Therefore, exact solutions for these four unknowns (the equations obtained from Eq. (15) are consistent) or the least-square solutions (the equations obtained from Eq. (15) are inconsistent) can be obtained.

Next, we adopt $\mathbf{C}_2=\frac{1}{2}\left[\begin{smallmatrix}1 & 1\\ j & -j\end{smallmatrix}\right]$ which is in the codebook for transmission on two antenna ports in [30], as an example to show the calculation of $\mathbf{P}_1$ and $\mathbf{G}_e$ using B-IOP. By defining $\mu_1=\frac{\alpha b^{(1)}-k^{(3)}p_e^{(2)}}{p_e^{(1)}}p_1^{(12)}$, $\mu_2=\frac{\alpha b^{(2)}-k^{(4)}p_e^{(2)}}{p_e^{(1)}}p_1^{(12)}$, $\mu_3=k^{(3)}p_1^{(22)}$, and $\mu_4=k^{(4)}p_1^{(22)}$, Eq. (15) can be rewritten as:

$$\begin{bmatrix}1&0&1&0\\1&0&1&0\\0&1&0&1\\0&1&0&1\end{bmatrix}\begin{bmatrix}\mu_1\\\mu_2\\\mu_3\\\mu_4\end{bmatrix}=\begin{bmatrix}\frac{1}{2}-\alpha b^{(1)}\\\frac{1}{2}\\\frac{1}{2}j-\alpha b^{(2)}\\-\frac{1}{2}j\end{bmatrix}. \tag{16}$$

By applying the elementary row transformation on the augmented matrix of Eq. (16), we can have:

$$\mathbf{\Omega}=\begin{bmatrix}1&0&1&0&\frac{1}{2}-\alpha b^{(1)}\\0&0&0&0&\alpha b^{(1)}\\0&1&0&1&\frac{1}{2}j-\alpha b^{(2)}\\0&0&0&0&-j+\alpha b^{(2)}\end{bmatrix}. \tag{17}$$

Since the rank of the coefficient matrix in Eq. (16) is 2, while $\mathrm{rank}(\mathbf{\Omega})=4>2$, Eq. (16) is inconsistent. Therefore, no exact solution for Eq. (16) exists. To obtain the least-square solution for Eq. (16), we can apply Theorem 2 as follows.

Theorem 2 ([28]): Given a non-homogeneous linear equation set $\mathbf{Ax}=\mathbf{b}$, where $\mathbf{A}\in\mathbb{C}^{m\times n}$ and $\mathbf{b}\in\mathbb{C}^{n\times 1}$ are both known, and $\mathbf{x}\in\mathbb{C}^{n\times 1}$ is to be solved. The necessary and sufficient condition that $\mathbf{x}$ is the least square solution for $\mathbf{Ax}=\mathbf{b}$ is that $\mathbf{x}$ is the solution for the equation set $\mathbf{A}^H\mathbf{Ax}=\mathbf{A}^H\mathbf{b}$.

Then, the inner and outer precoders can be calculated as:

$$\mathbf{P}_1=\begin{bmatrix}\left[b^{(1)}-\frac{k^{(3)}(\mu_1 b^{(2)}-\mu_2 b^{(1)})}{\mu_1 k^{(4)}-\mu_2 k^{(3)}}\right]\frac{\alpha p_1^{(12)}}{\mu_1}+p_1^{(12)} & p_1^{(12)}\\ \alpha\left[\frac{\mu_1}{\mu_2}b^{(2)}-b^{(1)}\right]\left[\frac{\mu_1}{\mu_2}k^{(4)}-k^{(3)}\right]^{-1}+\frac{\mu_3}{k^{(3)}} & \frac{\mu_3}{k^{(3)}}\end{bmatrix}, \tag{18}$$

and

$$\mathbf{G}_e=\begin{bmatrix}\frac{\mu_1}{p_1^{(12)}} & k^{(3)}\\ \frac{\mu_2}{p_1^{(12)}} & k^{(4)}\end{bmatrix}. \tag{19}$$

where $p_1^{(12)}$, α, $k^{(3)}$, $k^{(4)}$, μ_3 and μ_4 can take various values, yielding different $\mathbf{P}_1$ and $\mathbf{G}_e$. Recall that $\mu_3=k^{(3)}p_1^{(22)}$ and $\mu_4=k^{(4)}p_1^{(22)}$, in the selection of μ_3 and μ_4, $k^{(3)}\mu_4=k^{(4)}\mu_3$ should be satisfied. The transmission performance of Tx_1–Rx_1 pair is independent of the value of $p_1^{(12)}$. It should be noted that some values of $k^{(3)}$ and $k^{(4)}$ may incur nonexistence of least square solutions for Eq. (15), e.g., when we set $k^{(3)}=k^{(4)}=0$, Eq. (15) becomes an inconsistent homogeneous equation, in such a case neither precise nor least-square solutions for Eq. (15) exist. Therefore, to avoid this situation, we can change $\mathbf{k}$, or $k^{(3)}$ and $k^{(4)}$ in this example, until satisfactory $\mathbf{P}_1$ and $\mathbf{G}_e$ are found.

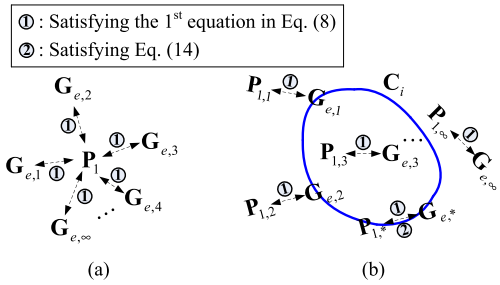

Fig. 3. Comparison of F-IOP and B-IOP. (a) F-IOP. (b) B-IOP.

Both F-IOP and B-IOP are based on the same principle adopting which of the inner ($\mathbf{P}_1$) and outer ($\mathbf{G}_e$) precoders can be obtained to differentiate multiple signals at their intended Rx while adjusting the overall effect of these signal components on the unintended Rx. However, the calculation of inner and outer precoders with the two IOP implementations is different. For F-IOP, $\mathbf{P}_1$ is determined first, then the general solution for $\mathbf{G}_e$ is obtained, and finally a particular $\mathbf{G}_e$ is selected out of all candidates. For B-IOP, it is codebook-aided with more weight on the performance of interfering transmission pair. With this scheme, a codeword, say $\mathbf{C}_i$, is first selected from the codebook as the design target of $\mathbf{G}_e\mathbf{P}_1$, and then $\mathbf{P}_1$ and $\mathbf{G}_e$ can be obtained by solving the equation $\mathbf{G}_e\mathbf{P}_1=\mathbf{C}_i$ simultaneously. Note that with B-IOP, the selected codeword $\mathbf{C}_i$ only provides a frame for the design of inner and outer precoders. Within this frame, there may exist various combinations of $\mathbf{P}_1$ and $\mathbf{G}_e$ satisfying Eq. (8), but we only adopt the one in accordance with the least-square criterion. That is, $\mathbf{C}_i$ cannot be employed directly as the precoder for $\mathbf{X}_1$ instead of $\mathbf{G}_e\mathbf{P}_1$, unless exact solutions for $\mathbf{P}_1$ and $\mathbf{G}_e$ of the equation $\mathbf{G}_e\mathbf{P}_1=\mathbf{C}_i$ exist.

We use Fig. 3 to illustrate the difference of F-IOP and B-IOP. As the figure shows, with F-IOP, $\mathbf{P}_1$ is fixed, while there are multiple solutions for $\mathbf{G}_e$ as long as the first equation in Eq. (8) is satisfied. The quality of solution, i.e., the spectral efficiency (SE) of Tx_1–Rx_1 pair, is determined by the values of α and $\mathbf{k}$. As for B-IOP, both $\mathbf{P}_1$ and $\mathbf{G}_e$ are flexible. Although there are multiple $\{\mathbf{P}_1,\mathbf{G}_e\}$ combinations satisfying the first equation in Eq. (8), only one, denoted by $\{\mathbf{P}_{1,*},\mathbf{G}_{e,*}\}$ that mostly matches the frame determined by $\mathbf{C}_i$ is selected, i.e., $\{\mathbf{P}_{1,*},\mathbf{G}_{e,*}\}=\arg\min_{\{\mathbf{P}_{1,n},\mathbf{G}_{e,n}\},n=1,2,\cdots}\|\mathbf{C}_i-\mathbf{G}_{e,n}\mathbf{P}_{1,n}\|$ where n is the index of the n^{th} B-IOP solution.

Based on the above discussions, B-IOP can be adopted as a supplementary of F-IOP.

Fig. 4 plots spatial spectrums of different signals at Rx_0 and Rx_1 with various IOP realizations. The experimental setup is

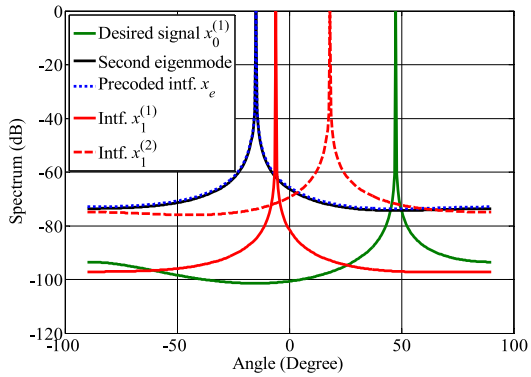

(a)

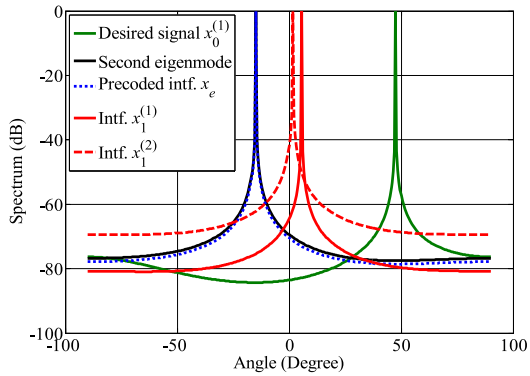

(b)

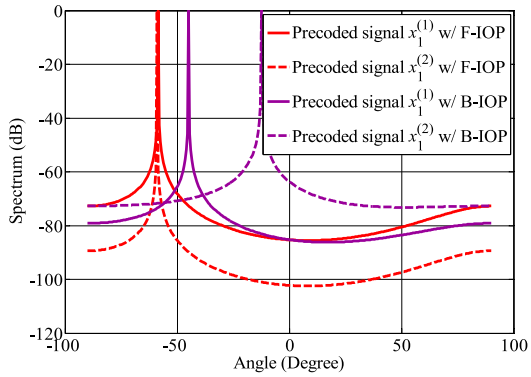

(c)

Fig. 4. Spatial spectrums of different signals with various IOP implementations. (a) Spatial spectrums at Rx_0 with F-IOP. (b) Spatial spectrums at Rx_0 with B-IOP. (c) Spatial spectrums at Rx_1.

identical to that of Fig. 2. Fig. 4(a) and (b) show the spatial spectrums perceived by Rx_0 with F-IOP and B-IOP. The desired signal of Rx_0 carrying $x_0^{(1)}$ is shown to occupy the principal eigenmode of $\mathbf{H}_0$, which is interfered with by the interfering signals from Tx_1, carrying $x_1^{(1)}$ and $x_1^{(2)}$, respectively. By applying F-IOP (Fig. 4(a)) or B-IOP (Fig. 4(b)) at Tx_1, the effective interference carrying x_e which can be either $x_1^{(1)}$ or $x_1^{(2)}$ is adjusted to the second eigenmode of $\mathbf{H}_0$. Therefore, the precoded effective interference is orthogonal to the desired transmission at Rx_0, i.e., both F-IOP and B-IOP can avoid interference to Rx_0. Fig. 4(c) plots the spatial spectrums of the signals pre-processed with F-IOP and B-IOP, respectively, at the intended Rx_1. The two signals precoded with F-IOP are shown to overlap with each other, and thus cannot be distinguished by their destination, Rx_1; whereas for B-IOP, the precoded signals are separable. In summary, in some situations the use of F-IOP may not be able to avoid interference to the unintended Rx while guaranteeing the interfering Tx–Rx pair's transmission performance. In such a case, B-IOP can be employed to manage multiple interferences from the same source.

V. Design of Reception of Interfering Tx–Rx Pair

From the previous design of IOP, we can see that the inner and outer precoders of both F-IOP and B-IOP rely on not only the channel status but also the transmitted symbols and the values of parameter vector $(\mathbf{k}, \alpha)$. Therefore, the intended Rx with respect to the interfering Tx cannot determine its receive filter without the knowledge of $(\mathbf{k}, \alpha)$ and the symbol information at the Tx side. We will thus propose a protocol to realize the synchronization of processing parameters at the interfering Tx and its intended Rx so that the Rx can adapt itself to the precoding strategy employed by the Tx.

Before presenting this reception design, we will first detail the block fading channel model mentioned in Section II. Based on this assumption, the synchronization between the interfering Tx and its Rx can be realized block by block.

The coherence time, denoted by τ_c, indicates the maximum length of time during which the channel remains unchanged. τ_c is approximately equal to the reciprocal of the maximum Doppler shift f_m, where $f_m = \frac{v f_0}{c}$. v denotes the user's speed and can be taken 3 km/h $-$ 20 km/h [30]. f_0 and c are the carrier frequency and speed of light, respectively. According to the LTE frequency allocation, we take $f_0 = 2.6$ GHz [30]. Moreover, we take the length of a time-slot as $T_s = 0.5$ ms [31]. So, we can have $f_m \approx 7.2$ Hz $-$ 48 Hz and $\tau_c \approx 21$ ms $-$ 139 ms, hence τ_c contains $\frac{\tau_c}{T_s} \approx 42 - 277$ time slots. In this paper, we assume the length of a block is approximately the same with that of the coherence time, and in the evaluation part we let a block contain 100 time slots (≈ 50 ms). Based on the above model, the interfering Tx and its intended Rx can operate with a period of the block-length. Parameter synchronization, as well as Rx side channel estimation and feedback to the associated Tx, are realized at the beginning of each block/cycle. After synchronization has been established, data transmission/reception of the interfering Tx–Rx pair can be carried out. However, provided with higher user's speed, e.g., 80 km/h $-$ 120 km/h, we can have $f_m \approx 192.6$ Hz $-$ 288.9 Hz and $\tau_c \approx 3.5$ ms $-$ 5.2 ms under $f_0 = 2.6$ GHz. Then, the number of time slots a block contains reduces to $\frac{\tau_c}{T_s} \approx 7 - 10$. In such a case, the variation of channel status becomes faster, yielding more stringent requirement for the timeliness of the abovementioned processing in a block.

First, we define data structures maintained at the interfering Tx and its intended Rx (referred to as interfering Rx for simplicity), respectively, as given in Fig. 5. For simplicity, we take BPSK and $K = 2$ as an example. Without loss of generality, we let the first transmitted symbol be the referential symbol as discussed in Section III-A.

Transmitted symbols	CSI	$(\mathbf{k},\alpha,\text{Flag})$	PMI	Count
(1,1) or (−1,−1)	$\mathbf{H}_0,\mathbf{H}_{10},\mathbf{H}_1$	Initial value	$f(\mathbf{H}_1)$	0
(1,−1) or (−1,1)		Initial value		0

(a)

Transmitted symbols	CSI	$(\mathbf{k},\alpha,\text{Flag})$	PMI
(1,1) or (−1,−1)	$\mathbf{H}_0,\mathbf{H}_{10},\mathbf{H}_1$	TBD	$f(\mathbf{H}_1)$
(1,−1) or (−1,1)		TBD	

(b)

Fig. 5. Data structures maintained at the interfering Tx–Rx pair. (a) Interfering Tx side. (b) Interfering Rx side.

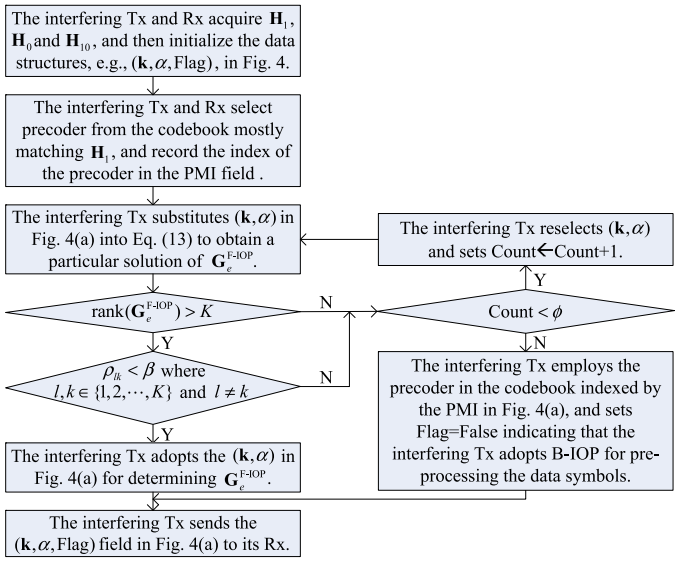

Fig. 6. Flowchart of synchronization phase of the interfering Tx–Rx pair.

When BPSK is employed and there are $K = 2$ interferences, four symbol combinations exist in the first column of Fig. 5. However, since the processing of symbol combinations (1,1) and $(-1,-1)$, as well as $(1,-1)$ and $(-1,1)$, are the same, the number of items of the structures can be reduced by a factor of $1/2$ [32]. According to Fig. 1, Rx_0 estimates $\mathbf{H}_0$ and $\mathbf{H}_{10}$, and then feeds them back to Tx_0, Tx_0 shares this information with Tx_1. In addition, Tx_1 obtains $\mathbf{H}_1$ from Rx_1's estimation. So, $\mathbf{H}_0$, $\mathbf{H}_{10}$ and $\mathbf{H}_1$ are filled in the CSI field of Fig. 5(a). Then, the interfering Tx_1 can use this information for determining inner and outer precoders. Moreover, Tx_1 should send Rx_1 $\mathbf{H}_0$ and $\mathbf{H}_{10}$ for calculation of the receive filter that can be referred to Eqs. (8) and (20) and the related discussions therein. Thus, the CSI field of Fig. 5(b) is identical to that of Fig. 5(a). In the third column of Fig. 5, the Flag is initialized to be True, indicating F-IOP is the default method. When Flag is set to False, B-IOP is adopted to determine $\mathbf{G}_e$.

The interfering Tx determines initial value of $(\mathbf{k},\alpha)$ for each transmitted symbol combination based on the description in Section III-C, and sets a counter for each row/item in the structure which is initialized to be 0 as shown in the last column in Fig. 5(a).

As discussed in Section III-C and the first paragraph in Section IV, we may need to attempt several times so as to obtain an appropriate $\mathbf{k}$ yielding feasible $\mathbf{G}_e$ with F-IOP, satisfying Claims 1 and 2, or even worse, under some channel realizations, F-IOP may be unavailable for any value of $(\mathbf{k},\alpha)$. In such a case, we need to set a counter for each row of Fig. 5(a). When the counter exceeds a preset threshold, say ϕ, and e.g., $\phi = 5$, we simply switch off F-IOP and adopt B-IOP. So that the timeliness of the proposed scheme can be guaranteed.

The $(\mathbf{k},\alpha)$ field at the Rx side is marked as TBD (To Be Determined) at the beginning of the synchronization phase, then it will be filled with the $(\mathbf{k},\alpha)$ value sent from the interfering Tx. In theory, the initial value of $(\mathbf{k},\alpha)$ can be arbitrary, but we find from a numerical simulation that under the system configurations of BPSK and two interferences, setting $(\mathbf{k},\alpha) = ([-\ -\ 0\ \frac{b^{(2)}}{p_e^{(2)}}]^T, 1)$, i.e., the outer precoder is a diagonal matrix, can yield higher spectral efficiency of the interfering Tx–Rx pair than that under other values of $(\mathbf{k},\alpha)$. So, we recommend use of this value for initialization.

One may have noticed that in Section IV, variable $\boldsymbol{\mu} = [\mu_1\ \mu_2\ \mu_3\ \mu_4]^T$ is introduced to solve Eq. (14). However, $\boldsymbol{\mu}$ is not necessary since in practice an iterative algorithm can also be used to solve Eq. (14). So, $\boldsymbol{\mu}$ is omitted in the third column of Fig. 5.

PMI (Precoding Matrix Indicator) in the fourth column indicates the index of precoder in the codebook [33] employed by the B-IOP. PMI can be determined by Tx_1 and Rx_1 individually, based on $\mathbf{H}_1$ (see $f(\mathbf{H}_1)$ in the PMI field of Fig. 5) in the synchronization phase. It should be noted that when B-IOP is adopted, the $(\mathbf{k},\alpha)$ value in the third column of Fig. 5 may have been updated ϕ times while applying F-IOP. In our design, $(\mathbf{k},\alpha)$ is reset to the initial value in using B-IOP since such a value can yield better SE.

Based on the above description, we plot in Fig. 6 the flowchart of synchronization for the interfering Tx–Rx pair. Note that the execution shown in the figure is in terms of each item/row of the structures in Fig. 5. For clarity, we use $\mathbf{G}_e^{\text{F-IOP}}$ to denote the outer precoder obtained with F-IOP. After establishing the synchronization, the Rx side processing can adapt to the precoding scheme, i.e., F-IOP or B-IOP, employed by the Tx.

For each symbol combination, there could be three possible situations during the determination of $(\mathbf{k},\alpha,\text{Flag})$, as given in Table I, which can be further used for determining the outer precoder. In the third line of the table, when the Flag in the $(\mathbf{k},\alpha,\text{Flag})$ field is set to False, a cascaded precoder with B-IOP, denoted by $\mathbf{G}_e^{\text{B-IOP}}\mathbf{P}_1^{\text{B-IOP}}$, is selected from the codebook based on the information in the PMI field. After establishing the synchronization, the $(\mathbf{k},\alpha,\text{Flag})$ fields at both the Tx and Rx side are the same. Then, the interfering Rx can employ a proper reception scheme adapting to the precoding method used by the Tx in decoding the corresponding desired symbols.

The above discussion takes BPSK and $K = 2$ as an example. In practice, the size (number of rows) of the structures depends on the modulation order at the Tx side and the number of interfering signals K cooperatively. Defining the k^{th} interference employs L_k-order modulation scheme, the size of the structures (without reduction) in Fig. 5 can then be calculated as

TABLE I
THREE SITUATIONS IN DETERMINING $(\mathbf{k}, \alpha, \text{FLAG})$ AT THE INTERFERING TX AND RX

Case	Descriptions
1	$\mathbf{G}_e^{\text{F-IOP}}$ obtained with initial value of $(\mathbf{k}, \alpha, \text{Flag})$ satisfies Claims 1 and 2. Flag = True.
2	The interfering Tx attempts $n < \phi$ times to find a proper $(\mathbf{k}, \alpha)$ yielding $\mathbf{G}_e^{\text{F-IOP}}$ which satisfies Claims 1 and 2. Flag = True.
3	No proper $(\mathbf{k}, \alpha)$ for feasible $\mathbf{G}_e^{\text{F-IOP}}$ has been found as $n = \phi$, then Flag = False and B-IOP is adopted.

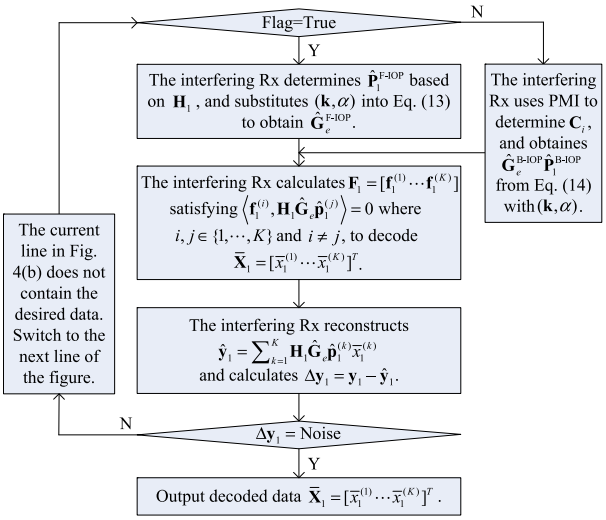

Fig. 7. Flowchart of the reception of the interfering Tx– pair.

$\prod_{k=1}^{K} L_k$. When BPSK ($L_k = 2$) is employed and $K = 2$, we have $\prod_{k=1}^{K} L_k = 4$. However, since some symbol combinations are processed in the same way, the number of items of the structures can be reduced by a factor of $1/2$ [32].

Since the necessary reception parameters along with the corresponding symbol combinations are provided, the receive filter can be computed at the interfering Rx side. Then, a reception mechanism given in Fig. 7 which is similar to that in [32], can be used to decode the desired data. In the flowchart, $\hat{\mathbf{P}}_1$ and $\hat{\mathbf{G}}_e$ denote the possible inner and outer precoders determined by the $(\mathbf{k}, \alpha, \text{Flag})$ field in Fig. 5(b) at the Rx side. Since $\hat{\mathbf{P}}_1$ and $\hat{\mathbf{G}}_e$ may not be the exact precoders $\mathbf{P}_1$ and $\mathbf{G}_e$ adopted by the Tx, we use $\hat{}$ to distinguish them. When Flag = True, $\hat{\mathbf{P}}_1$ and $\hat{\mathbf{G}}_e$ are specified as $\hat{\mathbf{P}}_1^{\text{F-IOP}}$ and $\hat{\mathbf{G}}_e^{\text{F-IOP}}$, respectively, while Flag = False corresponds to $\hat{\mathbf{P}}_1^{\text{B-IOP}}$ and $\hat{\mathbf{G}}_e^{\text{B-IOP}}$.

The processing procedure demonstrated in Fig. 7 is in terms of each row in Fig. 5(b). That is, given certain line in Fig. 5(b), either $\hat{\mathbf{P}}_1^{\text{F-IOP}}$ and $\hat{\mathbf{G}}_e^{\text{F-IOP}}$, or $\hat{\mathbf{G}}_e^{\text{B-IOP}}$ and $\hat{\mathbf{P}}_1^{\text{B-IOP}}$ are firstly calculated. Then, based on these precoders, the receiving filer $\mathbf{F}_1$ can be determined so as to decode data information $\mathbf{X}_1$ from the received mixed signal. Recall that IOP is the interfering Tx side operation and can thus be adapted to various reception schemes, such as ZF, minimum mean square error (MMSE), and matched filter (MF). Therefore, without loss of generality, as Fig. 7 shows, we employ ZF reception in our design. Next, the interfering Rx reconstructs signal based on $\mathbf{H}_1$, $\hat{\mathbf{G}}_e$, $\hat{\mathbf{P}}_1$, and the decoded $\bar{\mathbf{X}}_1$, and then subtracts the reconstructed signal $\hat{\mathbf{y}}_1$ from the received $\mathbf{y}_1$ to obtain $\Delta\mathbf{y}_1$. If only noise is outputted, the desired date is $\bar{\mathbf{X}}_1$, otherwise, the current line in Fig. 5(b) does not contain the desired data, so that we should move to the next row of the structure and return to the top of the flowchart to start a new processing.

VI. NUMERICAL RESULTS

We now evaluate the feasibility and SE performance of the proposed IOP schemes via MATLAB simulation. At first, we set $N_{T_i} = N_{R_i} = 2$ where $i = 0, 1$ and let Tx_1 transmit $K = 2$ data streams to Rx_1, thus incurring 2 interferences to Rx_0. An equal power is allocated to each of the streams. The transmitted symbols of Tx_1 are generated by using BPSK modulation, i.e., $x_1^{(1)}$ and $x_1^{(2)}$ are either 1 or -1. The interfered Tx_0–Rx_0 pair employs SVD-based pre-processing to send one data stream to Rx_0, i.e., applying SVD to $\mathbf{H}_0$ to obtain $\mathbf{H}_0 = \mathbf{U}_0\mathbf{\Sigma}_0\mathbf{V}_0^H$ and adopting $\mathbf{p}_0^{(1)} = \mathbf{v}_0^{(1)}$ where $\mathbf{v}_0^{(1)}$ is the first column of the right singular matrix $\mathbf{V}_0$. Therefore, there is only one DoF available for placing interfering components at Rx_0. In such a case, neither ZFBF nor IA is applicable due to the fact that both methods manage interferences individually, and hence require K DoFs for placing the adjusted interfering components. So, only SE of the proposed schemes is studied. Moreover, since IOP can avoid interference to the desired transmission to the interfered Rx_0, we only investigate the SE of the interfering Tx_1–Rx_1 pair.

Before presenting the simulation results, we first show how to calculate the SE of Tx_1–Rx_1 pair with IOP. As for F-IOP, since the inner-precoder $\mathbf{P}_1$ should be determined first, we adopt $\mathbf{P}_1 = \mathbf{V}_1$ as an example where $\mathbf{V}_1$ is the right singular matrix of $\mathbf{H}_1$. Since the optimal selection of the target codeword is more complex computationally, we employ fixed $\mathbf{C}_2$ in the simulation of B-IOP and the adoption of B-IOP in the Mixed-IOP $\mathbf{C}_2 = \frac{1}{2}\begin{bmatrix} 1 & 1 \\ j & -j \end{bmatrix}$ as the target codeword for $N_{T_1} = 2$. However, such simplification will incur mismatches between the precoder and the actual channel condition, thus degrading the transmission quality of the interfering Tx–Rx pair.

According to the reception design given in Section V, for the correct row in Fig. 5(b) containing the desired data symbols, we let $\mathbf{F}_1 = [\mathbf{f}_1^{(1)}\ \mathbf{f}_1^{(2)}]$ denote the receive filter matrix of ZF, then $\langle \mathbf{f}_1^{(1)}, \mathbf{H}_1\mathbf{G}_e\mathbf{p}_1^{(2)} \rangle = 0$ and $\langle \mathbf{f}_1^{(2)}, \mathbf{H}_1\mathbf{G}_e\mathbf{p}_1^{(1)} \rangle = 0$ should hold. The post-processed signal at Rx_1 is expressed as:

$$\bar{\mathbf{y}}_1 = \mathbf{F}_1^H\mathbf{H}_1\mathbf{G}_e\mathbf{p}_1^{(1)}x_1^{(1)} + \mathbf{F}_1^H\mathbf{H}_1\mathbf{G}_e\mathbf{p}_1^{(2)}x_1^{(2)} + \mathbf{F}_1^H\mathbf{n}_1. \quad (20)$$

Thus, the SE of Tx_1–Rx_1 pair can be calculated as:

$$R_1 = \sum_{i=1}^{2} \log_2 \left\{ 1 + \frac{\frac{P_T}{2} \| [\mathbf{f}_1^{(i)}]^H \mathbf{H}_1\mathbf{G}_e\mathbf{p}_1^{(i)} \|^2}{\sigma_n^2} \right\}. \quad (21)$$

Fig. 8 shows the average SE of the interfering Tx_1–Rx_1 pair with various IOP implementations, including F-IOP, B-IOP and Mixed-IOP (switching to B-IOP when F-IOP is inapplicable). As

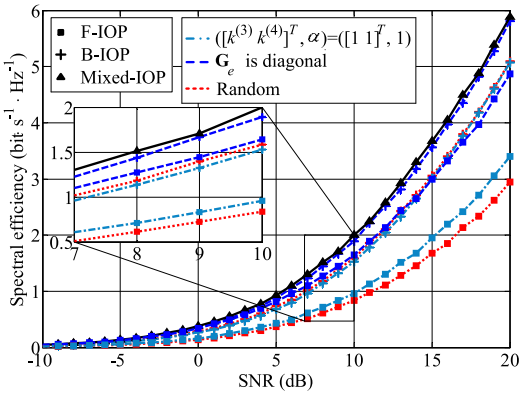

Fig. 8. SE of different IOP schemes under various $([k^{(3)}\ k^{(4)}]^T, \alpha)$ values.

for the simulation of F-IOP, the precoder $\mathbf{G}_e$ is calculated without verifying with Claims 1 and 2. In such a case, if the output $\mathbf{G}_e$ is invalid, i.e., yielding SE $= 0$, SE with F-IOP is counted as 0. In practice, we can employ a proper β when applying F-IOP so as to guarantee the quality of the resultant $\mathbf{G}_e$. The smaller β, the better $\mathbf{G}_e$, but a greater sacrifice of timeliness of F-IOP. Of the above three schemes, the first two are studied under two particular $([k^{(3)}\ k^{(4)}]^T, \alpha)$ settings, i.e., $([1\ 1]^T, 1)$ and $([0\ \frac{b^{(2)}}{p_e^{(2)}}]^T, 1)$. Note that the latter leads to $\mathbf{G}_e = \text{diag}([\frac{b^{(1)}}{p_e^{(1)}}\ \frac{b^{(2)}}{p_e^{(2)}}])$ determined cooperatively by $\mathbf{H}_{10}$, $\mathbf{H}_0$ and $\mathbf{P}_1$. Moreover, for a comprehensive comparison, we also simulated the average SE of F-IOP and B-IOP under 10^4 randomly generated $([k^{(3)}\ k^{(4)}]^T, \alpha)$ values. Each $([k^{(3)}\ k^{(4)}]^T, \alpha)$ sample is dependent on the channel realization and the transmitted symbols. As for the Mixed-IOP, we employ $([0\ \frac{b^{(2)}}{p_e^{(2)}}]^T, 1)$ which yields a diagonal $\mathbf{G}_e$ as the initial value of $([k^{(3)}\ k^{(4)}]^T, \alpha)$, and set $\beta = 0.2$ and $\phi = 5$. Moreover, when B-IOP is adopted, we reset $(\mathbf{k}, \alpha)$ in the third column of Fig. 5 to the initial value $([0\ \frac{b^{(2)}}{p_e^{(2)}}]^T, 1)$ so as to achieve statistically better SE. As the figure shows, given a particular IOP scheme (i.e., F-IOP or B-IOP), the SE under diagonal $\mathbf{G}_e$ obtained by letting $([k^{(3)}\ k^{(4)}]^T, \alpha) = ([0\ \frac{b^{(2)}}{p_e^{(2)}}]^T, 1)$, can lead to the highest SE compared to that with $([1\ 1]^T, 1)$ and averaged over 10^4 randomly-generated samples.

In the simulation of Fig. 8, we only studied various IOP realizations without comparing them with other existing schemes, because neither ZFBF nor IA is applicable when $N_{T_i} = N_{R_i} = 2$ where $i = 0, 1$, and $K = 2$. The pre-processing matrix under ZFBF, denoted by $\mathbf{P}^{ZFBF}$, should be designed to be orthogonal to the interference channel $\mathbf{H}_{10}$, and hence $\mathbf{H}_{10}\mathbf{P}^{ZFBF} = \mathbf{0}$ should hold, where $\mathbf{0}$ is a zero column vector. Since $\mathbf{H}_{10} \in \mathbb{C}^{N_{R_0} \times N_{T_1}}$, the existence of a solution for $\mathbf{P}^{ZFBF}$ requires $\text{rank}(\mathbf{H}_{10}) = \min(N_{T_1}, N_{R_0}) < N_{T_1}$, i.e., $N_{T_1} > N_{R_0}$. Moreover, to make K signal components distinguishable at their intended receiver Rx_1, the inequality $N_{T_1} - N_{R_0} \geq K$ should hold. Therefore, ZFBF requires the satisfaction of $N_{T_1} \geq N_{R_0} + K$, making it infeasible under $N_{T_i} = N_{R_i} = 2$ and $K = 2$. Since IOP is applicable under $N_{T_1} \leq N_{R_0}$, IOP and ZFBF cannot be compared under a same condition. It should be noticed that with ZFBF, the K transmitted beams pre-processed with $\mathbf{P}^{ZFBF}$ at Tx_1 no longer match $\mathbf{H}_1$ as p2pMIMO does, but the orthogonality among the beams is still maintained, thus being free from co-channel interference (CCI). The inter-beam orthogonality of ZFBF is advantageous over IOP, however, ZFBF costs more DoFs. As discussed in the introduction part, IA is not applicable to the case of multiple interferences from the same source. Given K and M, if Rx_0 is equipped with $N_{R_0} \geq M + K$ antennas, multiple interferences from Tx_1 can be adjusted so that each interfering component may occupy one DoF at Rx_0, hence avoiding disturbance to the desired transmission to Rx_0. However, in such a case, the interfering signals are not compressed as in traditional IA, and thus we call it *pseudo-IA*. In summary, given the same K and M, IOP sacrifices the orthogonality of multiple interfering signals while guaranteeing certain communication performance of the interfering transmission pair. IOP consumes one DoF regardless of the number of interfering components. Both ZFBF and pseudo-IA require more antennas to be equipped with the interfering Tx_1 and interfered Rx_0, respectively, than IOP. Since pseudo-IA requires more antennas at the interfered Rx, it is not only expensive in the DoF cost but also impractical especially when the Rx is a mobile device. Moreover, as Fig. 8 shows, the Mixed-IOP outperforms both F-IOP and B-IOP.

VII. Conclusion

In this paper, we have proposed a new IM scheme, called *Inside-Out Precoding* (IOP), to manage multiple interferences from the same source. By exploiting inter-plays among wireless signals, multiple interfering components which have been pre-processed by an inner-precoder, are treated as an effective interference to which an outer-precoder is applied, so that multiple interferences can be compressed into one dimension at the interfered Rx while being distinguishable at their intended Rx. We have also presented two IOP realizations — forward IOP (F-IOP) and backward IOP (B-IOP) — and discussed their incorporation in practical use. Our in-depth analysis and simulation results have demonstrated that the proposed IOP can effectively manage multiple interferences from the same source while guaranteeing the interfering Tx–Rx pair's transmission performance. Moreover, IOP aims to manage multiple interferences from the same source. However, disturbances may come from different sources and intend to various destinations in practice. Although we may exploit collaborations among interferers to realize IOP cooperatively, a lot of cooperation overhead will be incurred. In this case, it is more suitable for each interfering Tx to adjust its own signal individually so that multiple interferences can be aligned in a compressed subspace at the interfered Rx with little cooperation cost.

Although the proposed IOP schemes can realize alignment of multiple interferences from the same source with only one DoF cost at the interfered Rx, they incur a lot of computational complexity in computing the outer-precoder. Moreover, the outer-precoder is dependent on the transmitted symbols, that is, various outer-precoders should be calculated for different symbol combinations. However, it should be noticed that given K interferences and L_k-order modulation for the k^{th} interference, there are totally $\frac{1}{2}\prod_{k=1}^{K} L_k$ symbol combinations. Therefore, in a channel block where the channel parameters remain constant,

the outer-precoder for each symbol combination is calculated only once. That is, if the channel varies slowly or/and $\frac{1}{2}\prod_{k=1}^{K} L_k$ is small, the computational complexity could possibly be acceptable. The detailed analysis of IOP's complexity and further design of IOP with less complexity/cost are beyond the scope of this paper, but these are important issues that need to be addressed, and thus are matters of our future inquiry.

Appendix A
Proof of Claim 1

According to Eq. (6), the received mixed signal at Rx_1 can be expressed as $\mathbf{y}_1 = \mathbf{H}_1\mathbf{G}_e\mathbf{P}_1\mathbf{X}_1 + \mathbf{n}_1$. By noting that $\text{rank}(\mathbf{H}_1) = \min(N_{T_1}, N_{R_1}) \geq K$ and $\text{rank}(\mathbf{P}_1) = K$, given $\text{rank}(\mathbf{G}_e) < K$, we can have $\text{rank}(\mathbf{H}_1\mathbf{G}_e\mathbf{P}_1) \leq \min\{\text{rank}(\mathbf{H}_1), \text{rank}(\mathbf{G}_e), \text{rank}(\mathbf{P}_1)\} = \text{rank}(\mathbf{G}_e)$. Thus, $\text{rank}(\mathbf{H}_1\mathbf{G}_e\mathbf{P}_1) < K$ holds. That is, the number of desired signals of Tx_1–Rx_1 pair, K is larger than the dimension of the available signal space, i.e., $\text{rank}(\mathbf{H}_1\mathbf{G}_e\mathbf{P}_1)$. In other words, since $\mathbf{H}_1\mathbf{G}_e\mathbf{P}_1 = [\mathbf{H}_1\mathbf{G}_e\mathbf{p}_1^{(1)} \cdots \mathbf{H}_1\mathbf{G}_e\mathbf{p}_1^{(K)}]$, when $\text{rank}(\mathbf{H}_1\mathbf{G}_e\mathbf{P}_1) < K$, the spatial signatures of signals carrying $x_1^{(1)}, \ldots, x_1^{(K)}$, determined by $\mathbf{H}_1\mathbf{G}_e\mathbf{p}_1^{(1)}, \ldots, \mathbf{H}_1\mathbf{G}_e\mathbf{p}_1^{(K)}$, respectively, are linearly correlated. Therefore, there is at least one signal carrying data, say $x_1^{(k)}$, whose spatial signature $\mathbf{e}_{\mathbf{H}_1\mathbf{G}_e\mathbf{p}_1^{(k)}}$ can be linearly represented by that of the other $K-1$ signals carrying $x_1^{(1)}, \ldots, x_1^{(k-1)}, x_1^{(k+1)}, \ldots, x_1^{(K)}$. In such a case, Rx_1 cannot de-correlate all the K signal components. Thus, Claim 1 follows. ■

Appendix B
Proof of Claim 2

Our idea of proving Claim 2 is to show that the undesired situation described in Claim 2 exists. Take $N_{T_1} = N_{R_1} = N_{R_0} = K = 2$ and $\mathbf{G}_e = \text{diag}([\frac{b^{(1)}}{p_e^{(1)}} \frac{b^{(2)}}{p_e^{(2)}}])$ obtained by setting $k^{(3)} = 0$, $k^{(4)} = \frac{b^{(2)}}{p_e^{(2)}}$ and $\alpha = 1$, as an example. $\text{diag}(\mathbf{x})$ denotes the diagonalization of vector $\mathbf{x}$. We assume BPSK modulation is employed by Tx_1 for sending $K = 2$ signals, and hence the modulated symbols, denoted by $x_1^{(1)}$ and $x_1^{(2)}$, respectively, can be either 1 or -1. Without loss of generality, we take $x_1^{(1)}$ as the referential symbol.

Since $\mathbf{H}_1 = [\begin{smallmatrix} h_1^{(11)} & h_1^{(12)} \\ h_1^{(21)} & h_1^{(22)} \end{smallmatrix}]$ and the inner precoder $\mathbf{P}_1 = [\begin{smallmatrix} p_1^{(11)} & p_1^{(12)} \\ p_1^{(21)} & p_1^{(22)} \end{smallmatrix}]$, $\mathbf{H}_1\mathbf{G}_e\mathbf{p}_1^{(1)} = [\begin{smallmatrix} \frac{b^{(1)}}{p_e^{(1)}} p_1^{(11)} h_1^{(11)} + \frac{b^{(2)}}{p_e^{(2)}} p_1^{(21)} h_1^{(12)} \\ \frac{b^{(1)}}{p_e^{(1)}} p_1^{(11)} h_1^{(21)} + \frac{b^{(2)}}{p_e^{(2)}} p_1^{(21)} h_1^{(22)} \end{smallmatrix}]$ and $\mathbf{H}_1\mathbf{G}_e\mathbf{p}_1^{(2)} = [\begin{smallmatrix} \frac{b^{(1)}}{p_e^{(1)}} p_1^{(12)} h_1^{(11)} + \frac{b^{(2)}}{p_e^{(2)}} p_1^{(22)} h_1^{(12)} \\ \frac{b^{(1)}}{p_e^{(1)}} p_1^{(12)} h_1^{(21)} + \frac{b^{(2)}}{p_e^{(2)}} p_1^{(22)} h_1^{(22)} \end{smallmatrix}]$ hold. We define $\varepsilon_1 = p_1^{(11)} - p_1^{(12)}$ and $\varepsilon_2 = p_1^{(21)} - p_1^{(22)}$. Since unit vectors $\mathbf{p}_1^{(1)}$ and $\mathbf{p}_1^{(2)}$ are the first two columns of the inner precoding matrix $\mathbf{P}_1$, ε_1 and ε_2 cannot be close to 0 simultaneously. Otherwise, $\langle \mathbf{p}_1^{(1)}, \mathbf{p}_1^{(2)} \rangle = 0$ will not hold. Here, we use the descriptions that complex variable ε_1 or ε_2 is close to 0 ($\to 0$) or tends to ∞ ($\to \infty$) to indicate both the real and imaginary parts of such a variable are close to 0 or tend to ∞, respectively. By substituting ε_1 and ε_2 into the expressions of $\mathbf{H}_1\mathbf{G}_e\mathbf{p}_1^{(1)}$ and $\mathbf{H}_1\mathbf{G}_e\mathbf{p}_1^{(2)}$, we can get $\mathbf{H}_1\mathbf{G}_e\mathbf{p}_1^{(1)} = [\begin{smallmatrix} \frac{b^{(1)}}{\varepsilon_1} p_1^{(11)} h_1^{(11)} + \frac{b^{(2)}}{\varepsilon_2} p_1^{(21)} h_1^{(12)} \\ \frac{b^{(1)}}{\varepsilon_1} p_1^{(11)} h_1^{(21)} + \frac{b^{(2)}}{\varepsilon_2} p_1^{(21)} h_1^{(22)} \end{smallmatrix}]$ and $\mathbf{H}_1\mathbf{G}_e\mathbf{p}_1^{(2)} = [\begin{smallmatrix} \frac{b^{(1)}}{\varepsilon_1} p_1^{(11)} h_1^{(11)} + \frac{b^{(2)}}{\varepsilon_2} p_1^{(21)} h_1^{(12)} - b^{(1)} h_1^{(11)} - b^{(2)} h_1^{(12)} \\ \frac{b^{(1)}}{\varepsilon_1} p_1^{(11)} h_1^{(21)} + \frac{b^{(2)}}{\varepsilon_2} p_1^{(21)} h_1^{(22)} - b^{(1)} h_1^{(21)} - b^{(2)} h_1^{(22)} \end{smallmatrix}]$. When $\varepsilon_1 \to 0$, we have $\frac{1}{\varepsilon_1} \to \infty$, so that $\mathbf{H}_1\mathbf{G}_e\mathbf{p}_1^{(1)} \approx [\frac{b^{(1)}}{\varepsilon_1} p_1^{(11)} h_1^{(11)} \; \frac{b^{(1)}}{\varepsilon_1} p_1^{(11)} h_1^{(21)}]^T \approx \mathbf{H}_1\mathbf{G}_e\mathbf{p}_1^{(2)}$ is obtained. Therefore, $|\langle \mathbf{e}_{\mathbf{H}_1\mathbf{G}_e\mathbf{p}_1^{(1)}}, \mathbf{e}_{\mathbf{H}_1\mathbf{G}_e\mathbf{p}_1^{(2)}} \rangle| \approx 1$ holds. Similarly, $\varepsilon_2 \to 0$ will lead to $|\langle \mathbf{e}_{\mathbf{H}_1\mathbf{G}_e\mathbf{p}_1^{(1)}}, \mathbf{e}_{\mathbf{H}_1\mathbf{G}_e\mathbf{p}_1^{(2)}} \rangle| \approx 1$. Although the above analysis is with $N_{T_1} = N_{R_1} = N_{R_0} = K = 2$, the same conclusion can be drawn with more general parameter settings. Thus, Claim 2 follows.

It should be noted that in the proof of Claim 2, we only provide an example satisfying $|\langle \mathbf{e}_{\mathbf{H}_1\mathbf{G}_e\mathbf{p}_1^{(l)}}, \mathbf{e}_{\mathbf{H}_1\mathbf{G}_e\mathbf{p}_1^{(k)}} \rangle| \approx 1$ where $l, k \in \{1, 2, \ldots, K\}$ and $l \neq k$. In practice, there may be various situations leading to $|\langle \mathbf{e}_{\mathbf{H}_1\mathbf{G}_e\mathbf{p}_1^{(l)}}, \mathbf{e}_{\mathbf{H}_1\mathbf{G}_e\mathbf{p}_1^{(k)}} \rangle| \approx 1$. For simplicity, we have not exhaustively enumerated undesirable cases in this paper. ■

References

[1] N. Yang, L. Wang, G. Geraci, M. Elkashlan, J. Yuan, and M. Di Renzo, "Safeguarding 5 G wireless communication networks using physical layer security," *IEEE Commun. Mag.*, vol. 53, no. 4, pp. 20–27, Apr. 2015.

[2] N. Cheng *et al.*, "Performance analysis of vehicular device-to-device underlay communication," *IEEE Trans. Veh. Technol.*, vol. 66, no. 6, pp. 5409–5421, Jun. 2017.

[3] C. Chen, B. Wang, and R. Zhang, "Interference hypergraph-based resource allocation (IHG-RA) for NOMA-integrated V2X networks," *IEEE IoT J.*, vol. 6, no. 1, pp. 161–170, Feb. 2019.

[4] M. Patra, R. Thakur, C. S. R. Murthy, "Improving delay and energy efficiency of vehicular networks using mobile femto access points," *IEEE Trans. Veh. Technol.*, vol. 66, no. 2, pp. 1496–1505, Feb. 2017.

[5] Z. Li, K. G. Shin, and L. Zhen, "When and how much to neutralize interference?" in *Proc. IEEE Intl. Conf. Comput. Commun.*, 2017, pp. 1–9.

[6] F. Tang, Z. Md. Fadlullah, N. Kato, F. Ono, and R. Miura, "AC-POCA: Anti-coordination game based partially overlapping channels assignment in combined UAV and D2D based networks," *IEEE Trans. Veh. Technol.*, vol. 67, no. 2, pp. 1672–1683, Feb. 2018.

[7] F. Tang, Z. Md. Fadlullah, B. Mao, and N. Kato, "An intelligent traffic load prediction based adaptive channel assignment algorithm in SDN-IoT: A deep learning approach," *IEEE Internet Things J.*, vol. 5, no. 6, pp. 5141–5154, Dec. 2018.

[8] L. Song, A. Hjorungnes, and M. R. Bhatnagar, "Pre-equalization and precoding design for frequency-selective fading channels," in *Proc. IEEE Int. Conf. Commun.*, 2008, pp. 4744–4748.

[9] F. Tang, Y. Kawamoto, N. Kato, and J. Liu, "Future intelligent and secure vehicular network towards 6 G: Machine-learning approaches," *Proc. IEEE*, vol. 108, no. 2, pp. 292–307, Feb. 2020.

[10] J. Chen, A. Singh, P. Elia, and R. Knopp, "Interference neutralization for separated multiuser uplink-downlink with distributed relays," in *Proc. Inf. Theory Appl. Workshop*, 2011, pp. 1–9.

[11] Z. Li, F. Guo, C. Shu, K. G. Shin, and J. Liu, "Dynamic interference steering in heterogeneous cellular networks," *IEEE Access*, vol. 6, pp. 28552–28562, 2018.

[12] Z. Li, Y. Liu, K. G. Shin, J. Liu, and Z. Yan, "Interference steering to manage interference in IoT," *IEEE Internet Things J.*, vol. 6, no. 6, pp. 10458–10471, Dec. 2019.

[13] T. Yoo and A. Goldsmith, "On the optimality of multiantenna broadcast scheduling using zero-forcing beamforming," *IEEE J. Sel. Areas Commun.*, vol. 24, no. 3, pp. 528–541, Mar. 2006.

[14] G. Bresler, D. Cartwright, and D. Tse, "Feasibility of interference alignment for the MIMO interference channel," *IEEE Trans. Inf. Theory*, vol. 60, no. 9, pp. 5573–5586, Sep. 2014.

[15] V. Ntranos, M. A. Maddah-Ali, and G. Caire, "Cellular interference alignment," *IEEE Trans. Inf. Theory*, vol. 61, no. 3, pp. 1194–1217, Mar. 2015.

[16] V. R. Cadambe and S. A. Jafar, "Interference alignment and degrees of freedom of the K-user interference channel," *IEEE Trans. Inf. Theory*, vol. 54, no. 8, pp. 3425–3441, Aug. 2008.
[17] M. A. Maddah-Ali, A. S. Motahari, and A. K. Khandani, "Communication over MIMO X channels: Interference alignment, decomposition, and performance analysis," *IEEE Trans. Inf. Theory*, vol. 54, no. 8, pp. 3457–3470, Aug. 2008.
[18] C. M. Yetis, T. Gou, S. A. Jafar, and A. H. Kayran, "On feasibility of interference alignment in MIMO interference networks," *IEEE Trans. Sig. Process.*, vol. 58, no. 9, pp. 4771–4782, Sep. 2010.
[19] C. Na, X. Hou, and A. Harada, "Two-cell coordinated transmission scheme based on interference alignment and MU-MIMO beamforming," in *Proc. IEEE Veh. Technol. Conf.*, 2012, pp. 1–5.
[20] B. Guler and A. Yener, "Uplink interference management for coexisting MIMO femtocell and macrocell networks: An interference alignment approach," *IEEE Trans. Wireless Commun.*, vol. 13, no. 4, pp. 2246–2257, Apr. 2014.
[21] R. S. Ganesan, H. Al-Shatri, A. Kuehne, T. Weber, and A. Klein, "Pair-aware interference alignment in multi-user two-way relay networks," *IEEE Trans. Wireless Commun.*, vol. 12, no. 8, pp. 3662–3671, Aug. 2013.
[22] S. Zhang, W. Sun, J. Liu, and N. Kato, "Physical layer security in large scale probabilistic caching: Analysis and optimization," *IEEE Commun. Lett.*, vol. 23, no. 9, pp. 1484–1487, Sep. 2019.
[23] B. Nourani, S. A. Motahari, and A. K. Khandani, "Relay-aided interference alignment for the quasi-static interference channel," in *Proc. IEEE Intl. Conf. Symp. Inf. Theory*, 2010, pp. 405–409.
[24] B. Shen and Z. Li, "Coexistent transmission and user scheduling for CR-MIMO system based on interference alignment and cancellation," in *Proc. Annu. Int. Symp. Pers., Indoor, Mobile Radio Commun.*, 2013, pp. 403–407.
[25] Z. Li, J. Chen, L. Zhen, S. Cui, K. G. Shin, and J. Liu ,"Coordinated multi-point transmissions based on interference alignment and neutralization," *IEEE Trans. Wireless Commun.*, vol. 18, no. 7, pp. 3347–3365, Jul. 2019.
[26] N. Liu, I. Maric, A. J. Goldsmith, and S. Shamai, "Capacity bounds and exact results for the cognitive Z-interference channel," *IEEE Trans. Inf. Theory*, vol. 59, no. 2, pp. 886–893, Feb. 2013.
[27] N. Zhao, X. Zhang, F. R. Yu, and V. C. M. Leung, "To align or not to align: Topology management in asymmetric interference networks," *IEEE Trans. Veh. Technol.*, vol. 66, no. 8, pp. 7164–7177, Aug. 2017.
[28] P. Cheng, Y. Zhang, and Z. Xu, *Matrix Theory*. Xi'an, China: Northwestern Polytechnical Univ. Press, 2006.
[29] A. Cordero, J. R. Torregrosa, and M. P. Vassileva, "Pseudocomposition: A technique to design predictor-corrector methods for systems of nonlinear equations," *Appl. Math. Computation*, vol. 218, no. 23, pp. 11496–11504, 2012.
[30] "LTE; Requirements for further advancements for evolved universal terrestrial radio access (EUTRA) (LTE-Advanced)," 3GPP, Sophia Antipolis, France, Tech. Rep. TR 36.913 Release 15, 2018.
[31] A. Ghosh, J. Zhang, J. G. Andrews, and R. Muhamed, *Fundamentals of LTE*. 1st ed., Englewood Cliffs, NJ, USA: Prentice-Hall, 2010.
[32] Z. Li, J. Ding, X. Dai, and S. G. Kang, "Exploiting interactions among signals to decode interfering transmissions with fewer receiving antennas," *Comput. Commun.*, vol. 136, pp. 63–75, 2019.
[33] "LTE; evolved universal terrestrial radio access (E-UTRA); physical layer procedures," 3GPP, Sophia Antipolis, France, Tech. Rep. TS 36.213 Release 8, 2009.

Zhao Li (Member, IEEE) received the B.S. degree in telecommunications engineering, the M.S. and Ph.D. degrees in communication and information systems from Xidian University, Xi'an, China, in 2003, 2006, and 2010, respectively. He is currently an Associate Professor with the School of Cyber Engineering, Xidian University. He worked as a Visiting Scholar and then as a Research Scientist in the Real-Time Computing Laboratory at the Department of Electrical Engineering and Computer Science, The University of Michigan, during 2013-2015. He has published over 40 technical papers at premium international journals and conferences, like IEEE IoT, Journal, IEEE TWC, IEEE INFOCOM, *Computer Communications, Wireless Networks*, and so on. His research interests include wireless communication, 5G communication systems, resource allocation, interference management, IoT, and physical layer security.

Yujiao Bai is currently a Master's student with the School of Telecommunications Engineering at Xidian University. Her research interests include wireless communication, resource allocation, and interference management.

Kang G. Shin (Life Fellow, IEEE) received the B.S. degree in electronics engineering from Seoul National University, Seoul, Korea, and the M.S. and the Ph.D. degrees in electrical engineering from Cornell University, Ithaca, New York, in 1970, 1976, and 1978, respectively. He is the Kevin and Nancy O'Connor Professor of Computer Science and Founding Director of the Real-Time Computing Laboratory with the Department of Electrical Engineering and Computer Science, The University of Michigan, Ann Arbor, Michigan. At Michigan, he has supervised the completion of 82 Ph.D.s and also chaired the Computer Science and Engineering Division for three years starting in 1991. From 1978 to 1982 he was on the faculty of the Rensselaer Polytechnic Institute, Troy, New York. His current research focuses on QoS-sensitive computing and networks as well as on embedded real-time and cyber-physical systems. He has authored/coauthored more than 900 technical articles (more than 330 of which are published in archival journals) and more than 30 patents or invention disclosures. He has also received numerous institutional awards and best paper awards. He is Fellow of ACM.

Zheng Yan (Senior Member, IEEE) received the B.Eng. degree in electrical engineering and the M.Eng. degree in computer science and engineering from the Xi'an Jiaotong University, Xi'an, China in 1994 and 1997, respectively, the second M.Eng. degree in information security from the National University of Singapore, Singapore in 2000, and the Licentiate of Science and the Doctor of Science in Technology in electrical engineering from Helsinki University of Technology, Helsinki, Finland in 2005 and 2007. She is currently a Professor with the Xidian University, Xi'an, China and a Visiting Professor with the Aalto University, Espoo, Finland. She authored more than 150 peerreviewed publications and solely authored two books. She is the inventor and co-inventor of over 50 patents and PCT patent applications. Her research interests are in trust, security and privacy, social networking, cloud computing, networking systems, and data mining. Prof. Yan serves as an Associate Editor of *Information Sciences, Information Fusion, IEEE Internet of Things Journal, IEEE Access Journal, JNCA, Security and Communication Networks*, etc. She is a Leading Guest Editor of many reputable journals including ACM TOMM, FGCS, IEEE Systems Journal, MONET, etc. She served as a steering, organization and program committee member for over 70 international conferences.

Hui Li (Member,IEEE) received the B.Sc. degree from Fudan University in 1990 and the M.Sc. and Ph.D. degrees from Xidian University in 1993 and 1998, respectively. In 2009, he was with the Department of ECE, University of Waterloo as a Visiting Scholar. Since 2005, he has been a Professor with the School of Telecommunications Engineering, Xidian University, China. His research interests include the areas of cryptography, security of cloud computing, wireless network security, and information theory. He served as the TPC cochair of ISPEC 2009 and IAS 2009, General cochair of E-Forensic 2010, ProvSec 2011, and ISC 2011.